Cell

Glycan shielding enables TCR-sufficient allogeneic CAR-T therapy

Graphical abstract

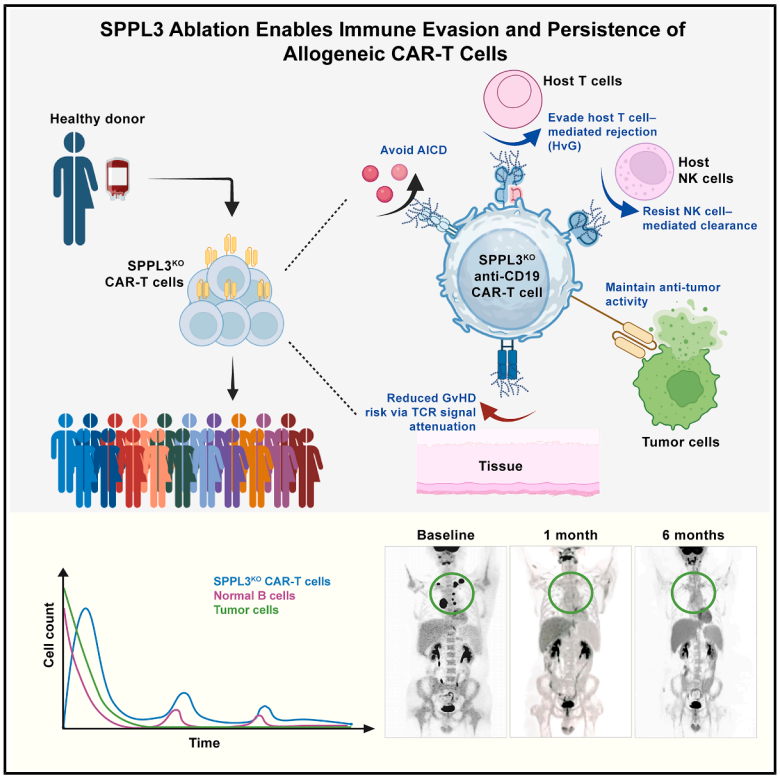

Highlights

- SPPL3 deletion increases the level and forms of glycosylation on primary T cells
- SPPL3 deletion reduces TCR expression, leading to reduced allogeneic immunity
- SPPL3 deletion does not impair tumor control by anti-CD19 allogeneic CAR-T cells
- SPPL3-null, TCR-sufficient anti-CD19 allogeneic CAR-T therapy is safe in three patients

Authors

Zeguang Wu, Jinhong Shi, Qiezhong Lamao, ..., Pengfei Yuan, Weidong Han, Wensheng Wei

Correspondence

pfyuan@edigene.com (P.Y.), hanwdrsw@163.com (W.H.), wswei@pku.edu.cn (W.W.)

In brief

SPPL3 deletion modifies glycosylation on primary T cells, reducing allogeneic immune responses without impairing tumor control by anti-CD19 allogeneic CAR-T cells. SPPL3-null, TCR-sufficient anti-CD19 allogeneic CAR-T therapy is safe in three patients with lymphoma or leukemia.

Wu et al., 2025, Cell *188*, 1–18
October 30, 2025
https://doi.org/10.1016/j.cell.2025.07.046

CellPress

Please cite this article in press as: Wu et al., Glycan shielding enables TCR-sufficient allogeneic CAR-T therapy, Cell (2025), https://doi.org/10.1016/j.cell.2025.07.046

Cell

CellPress
OPEN ACCESS

Article

Glycan shielding enables TCR-sufficient allogeneic CAR-T therapy

Zeguang Wu,[1,2,12] Jinhong Shi,[3,4,12] Qiezhong Lamao,[1,2,12] Yuanyuan Qiu,[1,12] Jinxin Yang,[1,12] Yang Liu,[4,12] Feifei Liang,[5,12] Xue Sun,[6,7] Wei Tang,[1] Changya Chen,[8,9] Qingming Yang,[4] Chunmeng Wang,[4] Zhifang Li,[4] Haixia Zhang,[5] Zhonghan Yang,[5] Yunyi Zhang,[5] Yuting Yi,[5] Xufen Zheng,[5] Yu Sun,[5] Kuiying Ma,[2] Lingling Yu,[2] Huihui Yang,[2] Zhaoxuan Wang,[1] Wenjuan Zheng,[1] Ling Yang,[5] Zhixuan Zhang,[1] Yongjian Zhang,[5] Zhiqiang Wu,[4] Yao Wang,[4] Catherine C.L. Wong,[7,10,11] Ming Jin,[5] Pengfei Yuan,[5,*] Weidong Han,[2,3,4,*] and Wensheng Wei[1,2,13,*]

[1]Biomedical Pioneering Innovation Center, Peking-Tsinghua Center for Life Sciences, Peking University Genome Editing Research Center, State Key Laboratory of Gene Function and Modulation Research, School of Life Sciences, Peking University, Beijing 100871, China
[2]Changping Laboratory, Beijing 102206, China
[3]School of Medicine, Nankai University, Tianjin 300071, China
[4]Department of Bio-Therapeutic, the First Medical Center, Chinese PLA General Hospital, Beijing 100039, China
[5]EdiGene Inc., Life Science Park, Changping District, Beijing 102206, China
[6]School of Pharmacy, University of Wisconsin-Madison, Madison, WI 53705, USA
[7]First School of Clinical Medicine, Peking University, Beijing 100871, China
[8]State Key Laboratory of Experimental Hematology, National Clinical Research Center for Blood Diseases, Haihe Laboratory of Cell Ecosystem, Institute of Hematology & Blood Diseases Hospital, Chinese Academy of Medical Sciences & Peking Union Medical College, Tianjin 300020, China
[9]Tianjin Institutes of Health Science, Tianjin 301600, China
[10]State Key Laboratory of Complex, Severe and Rare Diseases, Clinical Research Institute, Peking Union Medical College Hospital, Chinese Academy of Medical Science & Peking Union Medical College, Beijing 100730, China
[11]Tsinghua-Peking University Joint Center for Life Sciences, Tsinghua University, Beijing 100084, China
[12]These authors contributed equally
[13]Lead contact
*Correspondence: pfyuan@edigene.com (P.Y.), hanwdrsw@163.com (W.H.), wswei@pku.edu.cn (W.W.)
https://doi.org/10.1016/j.cell.2025.07.046

SUMMARY

Despite the success of autologous chimeric antigen receptor (CAR)-T cell therapy, achieving persistence and avoiding rejection in allogeneic settings remains challenging. We showed that signal peptide peptidase-like 3 (SPPL3) deletion enabled glycan-mediated immune evasion in primary T cells. SPPL3 deletion modified glycan profiles on T cells, restricted ligand accessibility, and reduced allogeneic immunity without compromising the functionality of anti-CD19 CAR molecules. In a phase I clinical trial, SPPL3-null, T cell receptor (TCR)-deficient anti-CD19 allogeneic CAR-T cells reached the safety primary endpoint, with grade 3 or higher cytokine release syndrome (CRS) observed in 3 out of 9 patients with relapsed/refractory B cell non-Hodgkin lymphoma (B-NHL) (ClinicalTrials.gov: NCT06014073). Reverse translational research highlighted the pivotal role of TCR in sustaining T cell persistence. We therefore evaluated the safety of SPPL3-null, TCR-sufficient CAR-T therapy on three patients with lymphoma or leukemia for compassionate care and observed no clinical signs of graft-versus-host disease. Our findings suggest glycan shielding by SPPL3 deletion is a promising direction for optimizing universal CAR-T therapies.

INTRODUCTION

Adoptive autologous chimeric antigen receptor (CAR)-T cell therapy has transformed the treatment landscape for aggressive B cell malignancies.[1–4] However, this groundbreaking therapy faces challenges in logistics, scalability, product quality, and patient eligibility.[5] To overcome these limitations, allogeneic CAR-T cell therapy has emerged as a promising alternative. Yet, this strategy faces formidable challenges, including host-versus-graft (HvG) immune rejection, limited *in vivo* persistence, and the risk of graft-versus-host disease (GvHD).

The primary challenge in utilizing allogeneic T cells stems from their inherent toxicity, principally driven by the potential for GvHD.[6,7] To counteract this danger, the vast majority of allogeneic CAR-T cells are engineered with T cell receptor (TCR) deletion strategies specifically designed to prevent GvHD.[8–10] In parallel, the limited persistence of allogeneic CAR-T cells is driven

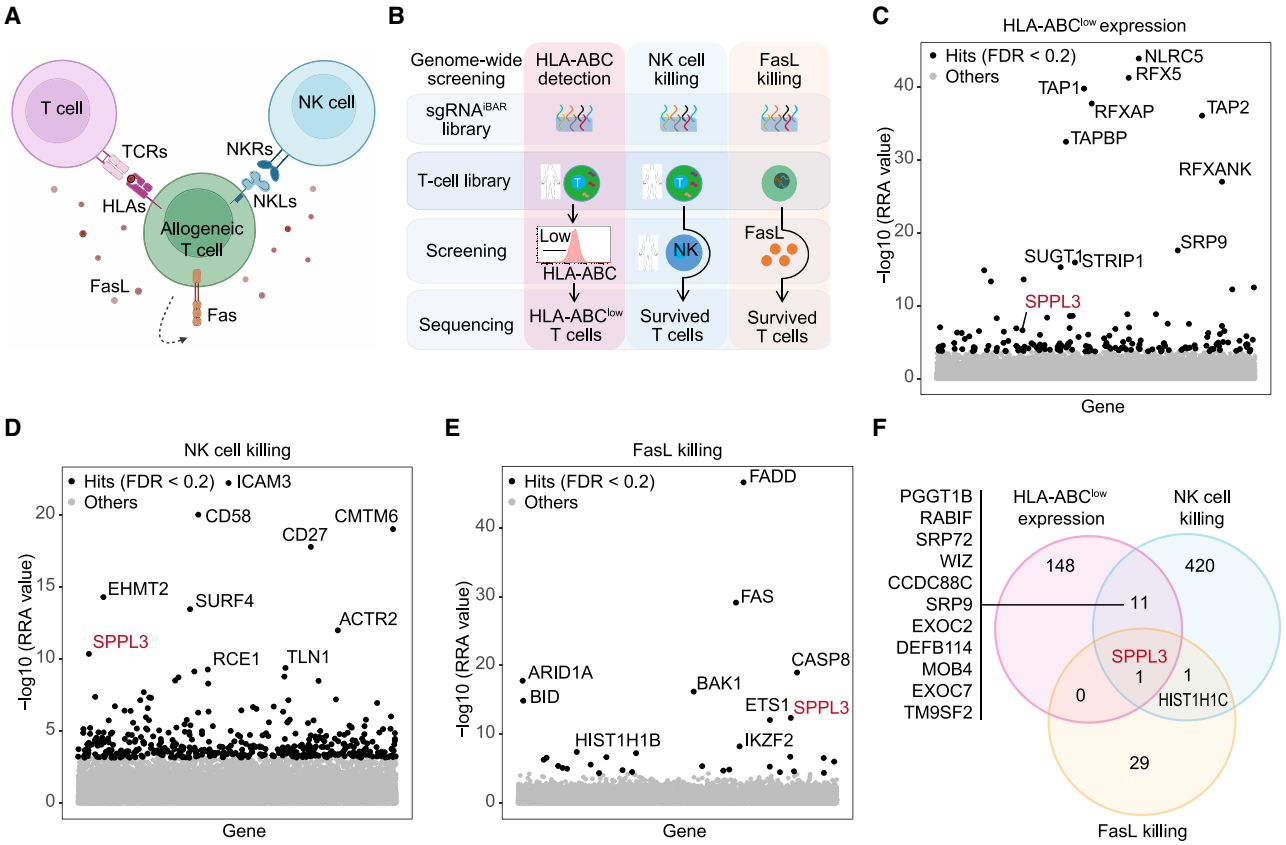

Figure 1. Genome-wide CRISPR-Cas9 screens in human T cells

(A) Schematic illustrating key effectors affecting persistence of allogeneic T cells.
(B) Unbiased approach for whole-genome screenings.
(C) Hits obtained from the HLA-ABC low expression screen.
(D) Hits obtained from the NK cell killing screen.
(E) Hits obtained from the FasL killing screen.
(F) Overlapping hits with a false discovery rate (FDR) < 0.2% from the three screens.
See also Figure S1.

by HvG responses from host T and natural killer (NK) cells as well as activation-induced cell death (AICD).[11–14] Genetic engineering strategies have been explored to improve immune evasion.[15] For instance, CD52 knockout enables CAR-T cells to resist alemtuzumab depletion.[9,16,17] Disrupting Beta-2 microglobulin (B2M) and human leukocyte antigen (HLA) molecules can reduce T cell-mediated HvG rejection,[7,18,19] though this simultaneously renders cells susceptible to NK cell attack via "missing self" recognition.[20–22] Notably, no current approach effectively addresses AICD in therapeutic T cells.

Our ability to explore genetic factors responsible for the endurance of allogeneic T cells has been limited by the lack of a comprehensive analytical framework.[23] Here, we utilized genome-wide CRISPR screening to identify signal peptide peptidase-like 3 (SPPL3) as a key regulator of glycosylation in human T cells. While SPPL3-mediated glycan remodeling has been implicated in tumor immune evasion,[24–27] its therapeutic potential in engineering immune-evasive CAR-T cells remains unexplored.

RESULTS

Identification of SPPL3 through genome-wide CRISPR screens in T cells

To identify genetic modifications that enhance the persistence of allogeneic T cells, we employed an unbiased genome-wide CRISPR screening approach in human T cells. Our hypothesis was that deleting specific genes could promote the desired T cell phenotype.[28–30] The main factors impeding the persistence of allogeneic T cells are host T and NK cell-killing mechanisms, which involve the activation of TCRs and NK receptors,[31] and AICD triggered by Fas-Fas ligand (FasL) interactions (Figure 1A).[10–13,32]

To identify genes whose deletions counteract T cell, NK cell, and AICD killing, we conducted genome-wide CRISPR screens in primary T cells using an optimized CRISPR library with single-guide RNA (sgRNA) and multiple internal barcodes (iBARs).[33–35] We generated human T cell libraries through lentiviral transduction of sgRNAs and electroporation of Cas9 mRNA,

Please cite this article in press as: Wu et al., Glycan shielding enables TCR-sufficient allogeneic CAR-T therapy, Cell (2025), https://doi.org/10.1016/j.cell.2025.07.046

CellPress
OPEN ACCESS

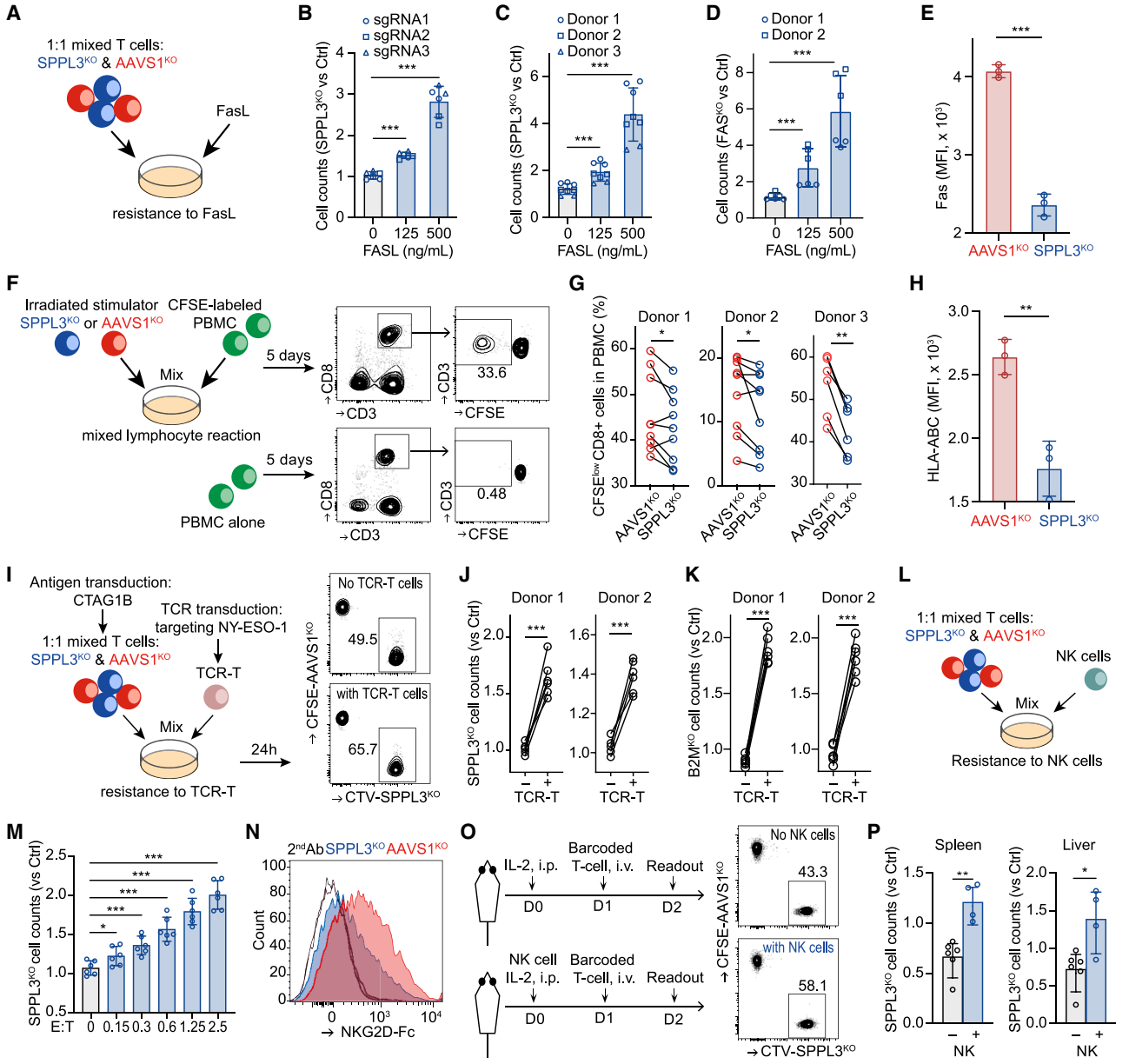

Figure 2. Resistance of *SPPL3*^{KO} primary T cells to FasL-induced cell death and T cell and NK cell killing

(A) Analysis of FasL-induced cell death in primary T cells. Flow cytometry was used to measure the percentage of *SPPL3*^{KO} cells.

(B) Accumulated data showing the results obtained using three sgRNAs targeting *SPPL3*.

(C) Accumulated data demonstrating the results obtained using three T cell donors.

(D) Analysis of FasL-induced cell death in *Fas*^{KO} T cells.

(E) Comparison of anti-Fas monoclonal antibody binding on *SPPL3*^{KO} and *AAVS1*^{KO} T cells.

(F) MLR settings. Irradiated *SPPL3*^{KO} or control cells (*AAVS1*^{KO}) were mixed with CFSE-labeled allogeneic PBMCs at an effector-to-target ratio of 5:1 for 5 days. Flow cytometry was used to evaluate the percentages of CFSE^{low} T cells among CD8^{+} T cells.

(G) Accumulated data obtained using 14 PBMC donors and three T cell donors.

(H) Comparison of anti-HLA-ABC monoclonal antibody binding on *SPPL3*^{KO} and *AAVS1*^{KO} T cells.

(I) Schematic of NY-ESO-1 TCR-T cell killing assay.

(J) Analysis of TCR-mediated killing against primary T cells. *SPPL3*^{KO} T cells were cultured with control cells (*AAVS1*^{KO}) in equal numbers and either treated with TCR-T cells or left untreated overnight.

(K) Analysis of TCR-mediated killing against *B2M*^{KO} T cells.

(L) Evaluation of allogeneic NK cells killing against activated T cells. *SPPL3*^{KO} and *AAVS1*^{KO} cells were incubated with NaP overnight. Subsequently, mixed cells were treated with purified NK cells or left untreated for 6 h.

(M) Accumulated data obtained with different E:T ratios. The data presented represent three donors.

(legend continued on next page)

followed by experimental assays to detect HLA-ABC expression, assess NK cell killing, and evaluate FasL-induced cell death. Deep sequencing determined the abundance of sgRNAs in the fractionated T cells compared with untreated cells (Figure 1B).

To investigate gene deletions that alleviate T cell recognition, we hypothesized that knocking out genes reducing HLA-I molecule abundance would impede TCR recognition and subsequent killing. To test this hypothesis, we isolated T cells with low surface intensity of HLA-A, -B, and -C subtypes (HLA-ABC) (Figure S1A). This screening identified NLR family CARD domain-containing protein 5 (NLRC5), the regulatory factor X (RFX) complex (RFX5, RFXAP, and RFXANK), the transporter associated with antigen processing (TAP) complex (TAP1 and TAP2), and TAP-binding protein (TABP) as top hits (Figure 1C).

By deleting the above specific gene targets, we aimed to reduce HLA-ABC expression to evade T cell targeting but also needed to address missing self-cytotoxicity by NK cells. To overcome this dual challenge of evading both T and NK cell recognition, we disrupted B2M in T cells to mimic low HLA-I expression (Figures S1B–S1D). Primary T cells transduced with the library were either propagated under normal conditions or challenged with expanded primary allogeneic NK cells. Specifically, the T cells were treated twice with NK cells, and viable B2M-negative T cells were selectively enriched (Figure S1E). This screening uncovered multiple gene candidates whose deletion in T cells conferred resistance to allogeneic NK cell killing (Figure 1D).

We used Jurkat T cells to screen for FasL-induced cell death due to their high Fas expression and sensitivity to FasL treatment.[36] The incubation duration and FasL concentrations were predetermined using annexin-V and DAPI staining (Figure S1F). Library-transduced Jurkat T cells were either grown under normal conditions or challenged with FasL treatment three times (Figure S1G). Among the enriched sgRNAs (Figure 1E), FAS (CD95), FAS-associated death domain protein (FADD), and caspase family (CASP)8 were identified as key nodes in apoptosis signaling.

Our comprehensive screens identified hundreds of genes with diverse functionalities, revealing previously undisclosed connections with allogeneic immune responses (Data S1). Of particular significance, *SPPL3* was identified as a common target gene. Its elimination in T cells resulted in resistance to NK cell killing, AICD, and reduced HLA-ABC detection (Figure 1F). SPPL3, a known Golgi-localized sheddase, regulates glycan formation and abundance by inhibiting glycosyltransferases and glycosidases.[37–39] Therefore, the ablation of *SPPL3* in cancer cells leads to altered glycan formation on the cell surface.[24,40,41] While this manuscript was in preparation, three independent studies reported that deleting *SPPL3* in cancer cells confers resistance to T cells, NK cells, neutrophils, and γδ T cells.[24,25,42] In line with these findings, we further showed that mutating functional residues in SPPL3 reduces tumor cell sensitivity to T cell-mediated cytotoxicity.[27]

Alleviating multiple effector-mediated immune clearance by editing SPPL3

To begin, we validated the protective effect of *SPPL3* ablation in Jurkat T cells against FasL-induced cell death in a dose-dependent manner (Figures S2A and S2B). We generated *SPPL3*^{KO} primary T cells and confirmed that the removal of SPPL3 does not increase human T cell proliferation, maintaining its viability as a gene editing target (Figures S2C and S2D). For universal T cells, we simultaneously ablated the TCR. We assessed the resistance of primary T cells to FasL-induced cell death using a competitive killing assay. *SPPL3*^{KO} T cells were labeled with Cell Trace Violet (CTV), while *AAVS1* knockout (*AAVS1*^{KO}) T cells were labeled with carboxyfluorescein succinimidyl ester (CFSE). These labeled cells were mixed at a 1:1 ratio for subsequent FasL treatments (Figure 2A). Our findings confirmed that *SPPL3*^{KO} primary T cells exhibited greater resistance to FasL-induced cell death than *AAVS1*^{KO} T cells across multiple sgRNAs targeting *SPPL3* and cells from different donors (Figures 2B and 2C). The assay showed consistent results, with *FAS*^{KO} T cells exhibiting resistance to FasL treatment (Figure 2D). Mechanistically, we observed reduced binding of the anti-Fas monoclonal antibody to *SPPL3*^{KO} T cells compared with control cells, suggesting impaired FasL binding on *SPPL3*^{KO} T cells (Figure 2E).

Previous studies have linked SPPL3 to HLA detection in cancer cells and the evasion of T cell killing.[24,43] Based on our screening results, we reasoned that *SPPL3*^{KO} T cells would have reduced interactions with allogeneic T cells (Figure 1C). To test this, we used a one-way mixed lymphocyte reaction (MLR), mixing irradiated *AAVS1*^{KO} or *SPPL3*^{KO} T cells with CFSE-labeled peripheral blood mononuclear cells (PBMCs) from allogeneic donors (Figure 2F). *AAVS1*^{KO} or *SPPL3*^{KO} T cells had their TCR expression disrupted and were purified as CD3-negative cells prior to the cultures. These T cells could be distinguished as $CD3^{-}CD5^{+}$ in the MLRs. T cells from PBMCs did not proliferate in the absence of allogeneic T cells. We quantified the stimulatory effects of irradiated T cells on allogeneic T cells by measuring the percentage of CFSE-negative T cells from PBMCs (Figure 2F). *SPPL3*^{KO} T cells had a diminished capacity to stimulate the proliferation of allogeneic T cells compared with *AAVS1*^{KO} T cells (Figure 2G). After confirming a reduced binding of anti-HLA-ABC monoclonal antibody to *SPPL3*^{KO} T cells (Figures 2H and S2E), we proposed that *SPPL3*^{KO} T cells could evade recognition by allogeneic T cells through the TCR-HLA axis. To directly assess the role of SPPL3 in TCR-mediated killing, we applied New York

(N) Comparison of anti-NKG2D-Fc antibody binding on *SPPL3*^{KO} (blue) and *AAVS1*^{KO} (red) T cells.
(O) Schematic representation of the experiment setup to evaluate NK cell killing against T cells *in vivo*.
(P) Evaluation of NK cell killing against T cells in the spleen and liver.
The data are representative of two independent experiments. Plots in (E), (H), and (N) reflect results from three independent experiments. Horizontal lines indicate the mean. Data in (B) ($n = 6$), (C) ($n = 8$), (D) ($n = 6$), (E) ($n = 3$), (G) ($n = 14$), (H) ($n = 3$), (J) ($n = 6$), (K) ($n = 6$), (M) ($n = 6$), and (P) ($n = 9$) are presented as mean ± SD. Statistical analyses were performed using the nonparametric Wilcoxon signed-rank sum test for (M), the Mann-Whitney U test for (B)–(D), (G), (J), (K), and (P), and unpaired t tests for all other comparisons. $^{*}p < 0.05$, $^{**}p < 0.01$, $^{***}p < 0.001$.
See also Figure S2.

Please cite this article in press as: Wu et al., Glycan shielding enables TCR-sufficient allogeneic CAR-T therapy, Cell (2025), https://doi.org/10.1016/j.cell.2025.07.046

esophageal squamous cell carcinoma 1 (NY-ESO-1)-specific TCR-T cells and transduced HLA-A2-positive T cells with cancer-testis antigen 1B (CTAG1B) (encoding NY-ESO-1) as targets (Figure 2I). Our results showed that *SPPL3*^{KO} T cells exhibited resistance to allogeneic TCR-T cell killing (Figures 2J and S2F). The same trend was observed with *B2M*^{KO} T cells, serving as a positive control (Figure 2K).

It is worth noting that low expression of HLA-ABC on target cells has been associated with increased sensitivity to NK cell targeting.[44] However, our screening results indicated that the elimination of *SPPL3* in T cells resulted in resistance to NK cell killing. We first used Jurkat T cells, a tumor cell line known to be susceptible to NK cell-mediated killing.[45] Despite the reduced binding of anti-HLA-ABC antibody to *SPPL3*^{KO} Jurkat T cells (Figure S2E), the absence of SPPL3 conferred protection against NK cell killing, suggesting that the resistance to NK cell killing is independent of B2M expression (Figure S2G). To increase the susceptibility of primary T cells to NK cell killing, we employed sodium propionate (NaP) treatment.[46] We performed a short-term killing assay using T and NK cells obtained from mismatched donors (Figure 2L). The results revealed that the elimination of SPPL3 conferred a dose-dependent protection to primary T cells against NK cell killing (Figure 2M). The consistent role of SPPL3 in conferring resistance to NK cell killing in both primary T cells and Jurkat T cells indicated its significant involvement in NK cell recognition rather than inhibition. Indeed, the deletion of *SPPL3* resulted in diminished binding of antibodies to ligands associated with all evaluated activating receptors on Jurkat T cells, as well as ligands of natural killer group 2D (NKG2D) on primary T cells (Figures 2N and S2H). Furthermore, we demonstrated that primary NK cells exhibited reduced killing of *SPPL3*^{KO} T cells in tissue settings (Figures 2O, 2P, and S2I).

We further evaluated the detection of HLA-II and CD58 on *SPPL3*^{KO} T cells, two key molecules involved in cell interactions.[47] Our results revealed a concentration-dependent variation in antibody detection, with reduced detection of HLA-II and increased detection of CD58 on *SPPL3*^{KO} T cells (Figures S2J and S2K). Additionally, we observed enhanced binding of soluble CD2 (Figure S2L).

Glycan analysis in primary T cells

To profile the substrates of SPPL3 in primary T cells, we hypothesized that these proteins would be enriched in *SPPL3*^{KO} T cells due to the lack of sheddase activity. Using mass spectrometry, we identified proteins with increased abundance in *SPPL3*^{KO} T cells compared with control T cells (Figure 3A; Data S2). Our analysis revealed multiple enzymes involved in glycosylation, observed in two donors (Figure 3B). The heightened expression of these enzymes indicates altered glycan patterns in *SPPL3*^{KO} T cells.[48] Indeed, we observed an elevated presence of N-Acetyl-D-lactosamine (LacNAc) and reduced levels of mannose on *SPPL3*^{KO} T cells, indicating an increased amount of complex N-glycans. Additionally, *SPPL3*^{KO} T cells also exhibited higher levels of sialic acid (Figure 3C), which plays a role in cell interactions, such as blood cell charge repulsion, due to its negative charge and hydrophilicity.[49] These results highlight the prevalence of complex N-glycans and sialic acid on *SPPL3*^{KO} T cells, potentially influencing immune effector recognition.

To gain insights into the glycan modifications of key molecules in *SPPL3*^{KO} T cells, specifically the natural TCR and synergistic CAR molecules, we mapped the glycan signature of the TCR/CD3 complex and the anti-CD19 CAR (Figure 3D). SPPL3 deletion increased the types and overall amount of glycans on the TCR/CD3 complex (Figures 3E and 3F). By contrast, the composition and abundance of glycans on the CAR molecule were comparable between edited and unedited cells (Figure 3G). We employed the conventional 18-amino-acid configuration for the CAR linker (Figure S2M), which lacks the Asn-X-Ser/Thr motif required for N-linked glycosylation. Consistent with the glycan analysis, the detection of the anti-CD19 CAR remained unaffected by *SPPL3* deletion, whereas TCR detection was significantly reduced on *SPPL3*^{KO} T cells (Figure 3H).

Effector functions of SPPL3^{KO}/TCR^{KO}/anti-CD19 CAR-T cells remain intact

We further characterized the dynamic transcriptome of CAR-T cells under repetitive stimulations, including *AAVS1*^{KO}, *SPPL3*^{KO}, TCR^{KO}, and *SPPL3*^{KO}/TCR^{KO} (Figure 4A). The clusters of transcripts were found to be enriched based on the number of stimulations rather than the genotype of the cells (Figure 4B). While *SPPL3*^{KO} cells exhibited an increased proliferation signature, no discernible differences were observed in pathways of cell activation, apoptosis, differentiation, or exhaustion (Figure 4C).

Functionally, the killing capacity of *SPPL3*^{KO}/TCR^{KO}/anti-CD19 CAR-T cells was comparable to that of control anti-CD19 CAR-T cells (Figure 4D). These cells exhibited a growth advantage over control cells during repetitive stimulations (Figure 4E). Since CAR-T cells are known to be susceptible to AICD upon repetitive antigen stimulations,[29] the enhanced expansion observed could be attributed to their reduced binding to FasL. Importantly, these cells showed a clear reliance on interleukin-2 for their growth (Figure 4F). These results collectively suggest that the effector functions of *SPPL3*^{KO}/anti-CD19 CAR-T cells remain intact.

SPPL3^{KO}/anti-CD19 CAR-T cells eliminated tumors *in vivo*

To evaluate the tumor control capacity of *SPPL3*^{KO}/TCR^{KO}/anti-CD19 T cells *in vivo*, we employed xenograft models bearing Nalm6 cells (Figure 4G). Mock T cells showed no tumor control (Figure 4H). *SPPL3*^{KO}/TCR^{KO}/anti-CD19 CAR-T cells expanded *in vivo*, significantly inhibited tumor growth, and improved animal survival, demonstrating survival rates comparable to control CAR-T cells at a dose of 6×10^6, while eliminating the tumor at a higher dose (Figures 4I and 4J).

We further assessed the expansion of *SPPL3*^{KO}/TCR^{KO}/anti-CD19 T cells under repetitive stress stimulations *in vivo* (Figure 4K). Although *SPPL3*^{KO} CAR-T cells inhibited tumor cells with similar efficiency to control CAR-T cells, we observed an increased number of CAR-T cells in the tumor rechallenge experiment (Figures 4L–4N).

SPPL3^{KO}/TCR^{KO}/anti-CD19 CAR-T cell therapy in B-NHL

Following promising preclinical results, a phase I clinical trial was initiated to evaluate the safety and tolerability of glycan-shield

Please cite this article in press as: Wu et al., Glycan shielding enables TCR-sufficient allogeneic CAR-T therapy, Cell (2025), https://doi.org/10.1016/j.cell.2025.07.046

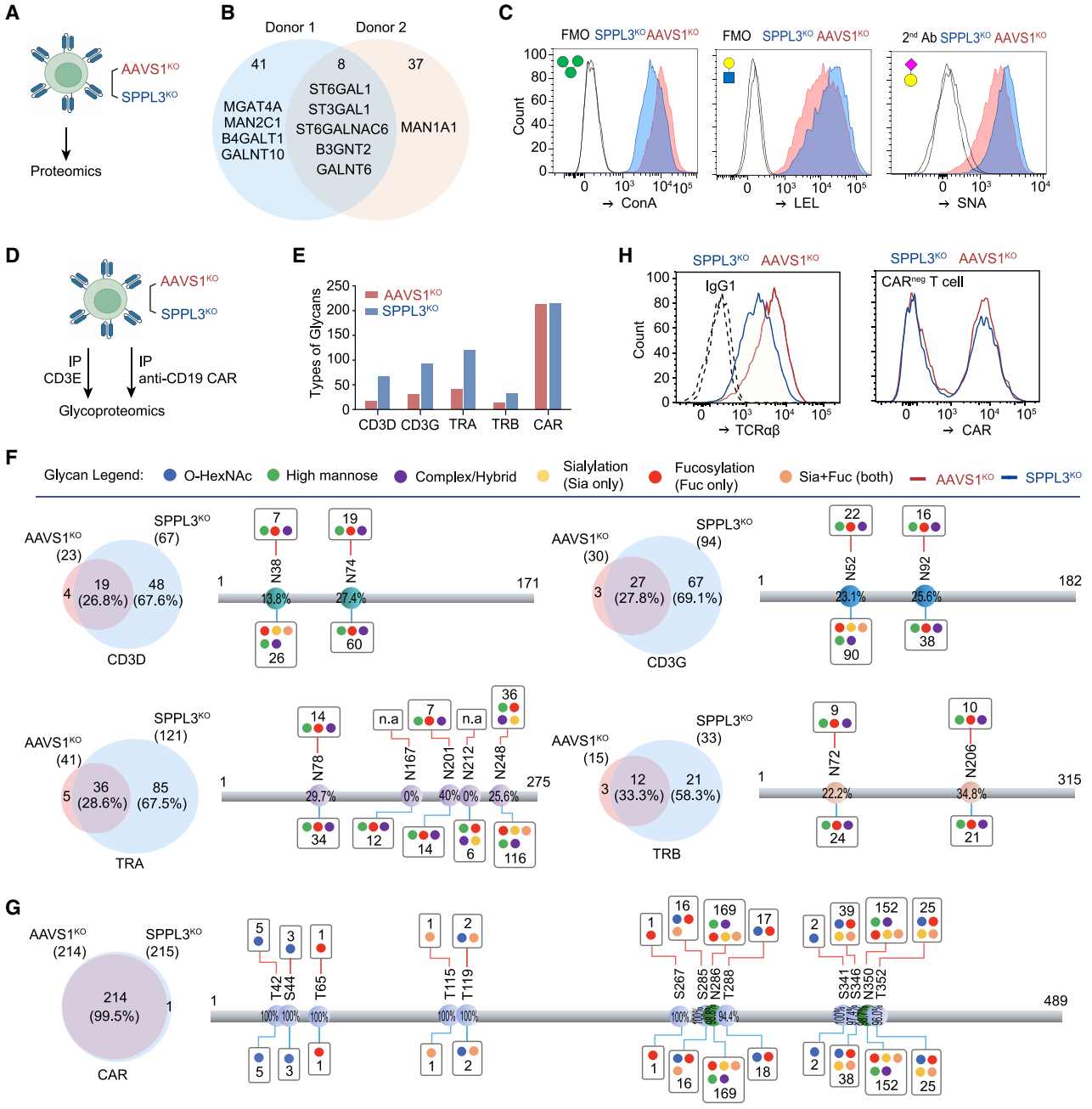

Figure 3. The detection of glycans on primary T cells

(A) Schematic representation of the experiment setup for proteomics analysis.

(B) Overlapping of proteins that were increased in *SPPL3*^{KO} T cells compared with control T cells.

(C) The binding of concanavalin A (ConA), Lycopersicon esculentum lectin (LEL), and Sambucus Nigra lectin (SNA) on *SPPL3*^{KO} and *AAVS1*^{KO} T cells. Staining controls are indicated as black lines. The plots are representative of two independent experiments using three T cell donors.

(D) Schematic representation of the experiment setup for glycoproteomics analysis.

(E) Glycosylation landscape of CD3D, CD3G, TRA, TRB, and CAR in *SPPL3*^{KO} and *AAVS1*^{KO} T cells.

(F) CD3D, CD3G, TRA, and TRB glycosylation analysis.

(G) CAR glycosylation profiling.

(H) Detection of TCRαβ and anti-CD19 CAR on *SPPL3*^{KO} and *AAVS1*^{KO} T cells. Staining controls are indicated as black lines. The plot shown is representative of three independent experiments.

Please cite this article in press as: Wu et al., Glycan shielding enables TCR-sufficient allogeneic CAR-T therapy, Cell (2025), https://doi.org/10.1016/j.cell.2025.07.046

CellPress
OPEN ACCESS

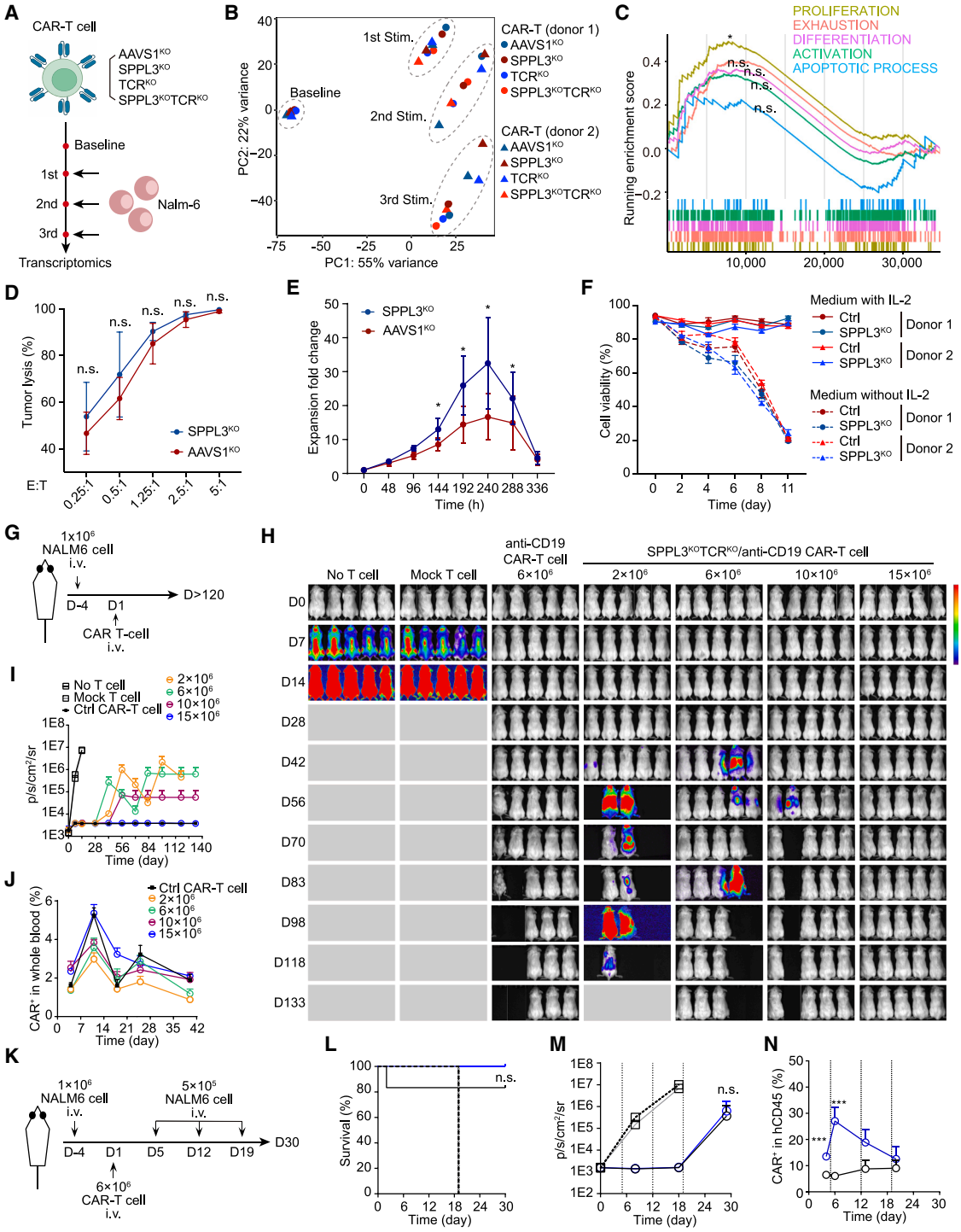

Figure 4. Functionality of *SPPL3*^{KO}/anti-CD19 CAR-T cells

(A) Schematic representation of the experiment setup for transcriptome analysis.

(B) Principal-component analysis (PCA) of RNA sequencing (RNA-seq) counts for 2,500 of the most dispersed genes.

(C) Gene set enrichment analysis (GSEA) of CAR-T cells comparing *SPPL3*^{KO}TCR^{KO} and *AAVS1*^{KO}TCR^{KO} cells. The running enrichment scores of gene sets are shown.

(D) Killing capacity of *SPPL3*^{KO}/TCR^{KO}/anti-CD19 and *AAVS1*^{KO}/TCR^{KO}/anti-CD19 CAR-T cells against Nalm6 cells.

(E) Expansion of *SPPL3*^{KO}/TCR^{KO}/anti-CD19 and *AAVS1*^{KO}/TCR^{KO}/anti-CD19 CAR-T cells in response to repetitive antigen challenges.

(F) IL-2-dependent growth of *SPPL3*^{KO}/anti-CD19 CAR-T cells.

(legend continued on next page)

Please cite this article in press as: Wu et al., Glycan shielding enables TCR-sufficient allogeneic CAR-T therapy, Cell (2025), https://doi.org/10.1016/j.cell.2025.07.046

CAR-T cell therapy in patients with relapsed/refractory (r/r) B cell non-Hodgkin lymphoma (B-NHL; NCT06014073). The protocol was approved by the ethics committee of the Chinese People's Liberation Army (PLA) General Hospital (Data S3). All the patients provided written informed consent in the study in accordance with the principles outlined in the Declaration of Helsinki before enrollment. The infusion of *SPPL3*^{KO}/TCR^{KO}/anti-CD19 CAR-T cells was administered as a single dose at escalating doses: 1×10^6/kg, 3×10^6/kg, and 10×10^6/kg using a classical 3+3 design (Figure S3A). The primary endpoints of the study were dose-limiting toxicities (DLTs) within 28 days and determining the recommended phase II dose (RP2D). Key secondary endpoints included objective response rate (ORR), complete response (CR) rate, pharmacokinetics, and pharmacodynamics (PKs/PDs) (Figure 5A; see STAR Methods for details).

A total of 9 subjects were enrolled and underwent *SPPL3*^{KO}/TCR^{KO}/anti-CD19 CAR-T infusion between September 6, 2023, and May 31, 2024 (Table S1). An additional case received compassionate use due to a history of autologous CAR-T treatment (Figure 5A). No DLTs or GvHD were observed within 28 days of CAR-T infusion. The most commonly observed adverse events (AEs) of any grade among all nine patients were lymphopenia, anemia, thrombocytopenia, and cytokine release syndrome (CRS). Grade 3 or higher CRS occurred in 3 patients (33%). CRS onset typically occurred 1 day after infusion (median range: 0.3–5 days) and lasted a median of 7 days (range: 5–9 days). Three patients (33%) experienced immune effector cell-associated neurotoxicity syndrome (ICANS), with one case being grade 1 and two cases being grade 3. ICANS onset occurred at a median of 5 days (range: 4–5 days) post-infusion, lasting a median of 3 days (range: 3–5 days) (Figures 5B, S3B, and S3C; Table S2). Levels of immune response-related cytokines peaked on day 6 and returned to normal within 10 days (Figures 5C, S3D, and S3E). The ORR among the 9 subjects was 100%, with a CR rate of 66.7% and a partial response (PR) rate of 33.3% (Figures 5D and 5E). As of December 31, 2024, the median duration of response was 2.2 months (range: 0.8–7.3 months), with three out of 9 subjects maintaining responses for over 6 months. Two patients exhibited CD19 loss or dimming post-infusion (Figures S3F and S3G). Three patients succumbed to disease progression, and one patient passed away from pulmonary infections with Enterobacter cloacae and influenza B virus 3 months after treatment.

The median peak CAR vector copy number (CAR-VCN) detected in peripheral blood was 123,529.4 copies/mg (range: 17,710.0–622,800.0) (Figure S3H). Median peak levels of CD3$^-$CAR$^+$ T cells reached 49.2 cells/mL (range: 4.5–675.9), and the median area under the curve (AUC) between days 0 and 28 ($AUC_{0–28}$) for CD3$^-$CAR$^+$ T cells was 104.5 cells/mL (range: 18.2–2,739.0) (Figure S3I). A comparative analysis of CAR-T cell expansion kinetics showed no significant differences between patients who experienced CRS/ICANS and those who did not (Figures S4A–S4E). Additional analysis revealed a positive correlation trend between CAR-T expansion and both cell dose and tumor burden as measured by sum of product diameters (SPDs) (Figures S4F–S4J). The median time to peak expansion of CD3$^-$CAR$^+$ T cells was 7 days post-infusion (range: 5–9). Based on the integrated assessment of safety, pharmacokinetics, and preliminary efficacy, the RP2D was established at 3×10^6 cells/kg, as determined by the safety review committee (SRC).

An intriguing observation from the trial was the significant expansion of residual CD3$^+$CAR$^+$ T cells in peripheral blood, despite the initial infusion product containing less than 0.3% CD3$^+$ cells. During bone marrow recovery, 7 of 10 patients (including one compassionate-use patient) exhibited expansion of residual CD3$^+$TCR$^+$ CAR-T cells. Notably, in 4 of these 7 patients, the expansion of CD3$^+$CAR$^+$ cells coincided with a lack of peripheral B cells. In one case (patient [Pt] 02), a neck lymphoma mass initially enlarged by day 68 but later underwent spontaneous reduction, softening, and collapse without additional anti-tumor intervention (Figure S4K). During this period, CD3$^+$TCR$^+$ CAR-T cells expanded, suggesting their potential role in monitoring tumor progression and contributing to long-term disease control. Remarkably, these TCR-sufficient CAR-T cells expanded over 100-fold after infusion and persisted for more than 2 months (Table S3). However, the limited number of CD3$^+$ CAR-T cells, possibly due to low initial input and significant expansion, was insufficient to sustain long-term B cell suppression (Figure 5F).

Interestingly, the peak number of CD3$^+$ CAR-T cells exceeded the internationally recognized threshold for residual T cells capable of triggering GvHD in allogeneic transplants (2E+5/kg; Table S3). Among patients with elevated CD3$^+$ CAR-T cells, 2 out of 7 developed mild skin rashes (Figure S4L). These rashes appeared around day 52 (range: 29–75 days) and lasted for approximately 17 days (range: 10–24 days), coinciding with the detectable presence of CD3$^+$ CAR-T cells. Classified as grade 1 skin reactions, these symptoms were self-limited. The absence of typical GvHD is likely due to attenuated TCR signaling resulting from *SPPL3* deletion (Figure 3H).

Phenotypic stability and long-term persistence of SPPL3^{KO}/anti-CD19 CAR-T cells *in situ*

Pt 11 presented with a substantial peritoneal tumor burden and accumulation of abdominal fluid. By day 6 post-infusion,

(G) Experimental design of (H)–(J).
(H) Bioluminescence imaging (BLI) images showing tumor burden (n = 5 per group).
(I) BLI signals from all groups are shown, including no T cell (dashed line), mock T cell (gray), and control anti-CD19 CAR-T cells (black).
(J) Percentage of anti-CD19 CAR-positive cells in the blood.
(K) Experimental design of (L)–(N).
(L) Kaplan-Meier plot depicting overall survival across all groups. No T cell (dashed line), mock T cell (gray), *SPPL3*^{KO}/TCR^{KO}/anti-CD19 CAR-T cells (blue), and anti-CD19 CAR-T cells (black) are shown.
(M) BLI signals of all groups (n = 6 per group). Dash lines indicate the dates of tumor cell injections.
(N) Percentage of anti-CD19 CAR-positive cells in the human CD45$^+$ cells. Dash lines indicate the dates of tumor cell injections. Horizontal lines indicate the mean in panels. t test was used to compare luciferase intensity of tumors. Mann-Whitney U test was performed for other analysis; $^*p < 0.05$, $^{**}p < 0.01$, $^{***}p < 0.001$.

Please cite this article in press as: Wu et al., Glycan shielding enables TCR-sufficient allogeneic CAR-T therapy, Cell (2025), https://doi.org/10.1016/j.cell.2025.07.046

CellPress
OPEN ACCESS

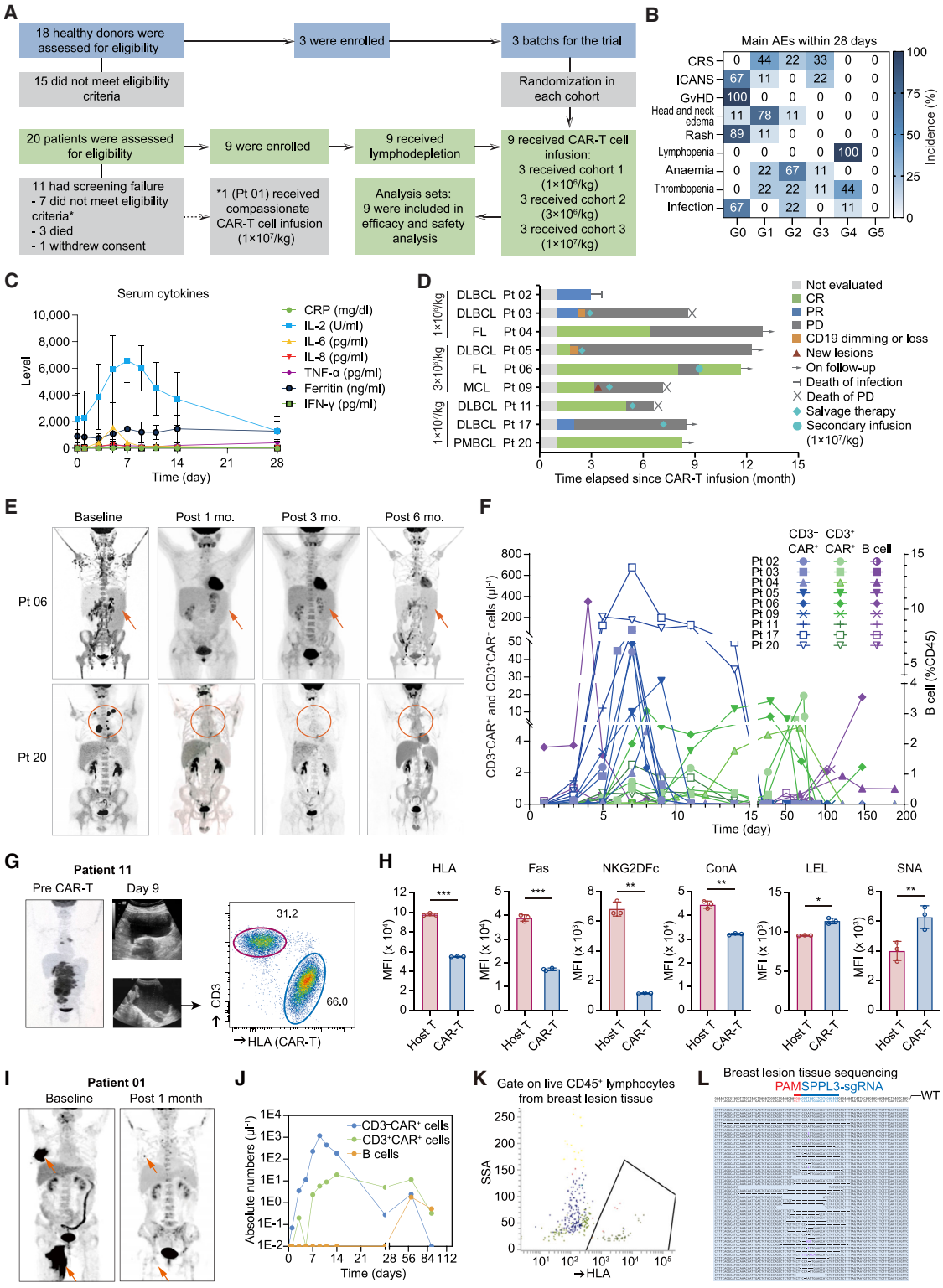

Figure 5. Clinical design, safety, response, expansion kinetics, and long-term persistence of SPPL3^{KO}/TCR^{KO}/anti-CD19 CAR-T therapy

(A) Study design: overview of the experimental design employed in the study.

(B) Incidence and frequency of main AEs observed within 28 days of the course of CAR-T therapy (n = 9).

(C) Detection and analysis of cytokine levels in patients undergoing CAR-T therapy.

(legend continued on next page)

Please cite this article in press as: Wu et al., Glycan shielding enables TCR-sufficient allogeneic CAR-T therapy, Cell (2025), https://doi.org/10.1016/j.cell.2025.07.046

CAR-T cell levels in the fluid reached 597 cells/μL (Figure 5G). Phenotypic analysis using donor-specific HLA antibody (Figures 5G and S4M) showed that these CAR-T cells (day 9) exhibited robust proliferation and effective tumor cell killing capacity in culture (Figures S4N and S4O). *In vivo* profiling revealed consistent expression of immune tolerance-associated molecules on glycan-shielded CAR-T cells (Figure 5H). Importantly, glycan shielding had no discernible impact on the detection of CD4 and CD8, suggesting minimal variation in protein levels between donors (Figure S4P).

Pt 01, who had previously undergone autologous CD19/CD20 CAR-T therapy, received compassionate therapy with *SPPL3*^{KO}/TCR^{KO}/anti-CD19 CAR-T cells at a dose of 10×10^6/kg after experiencing disease progression (Figure S5A). The patient had a high level of serum human anti-mouse antibodies (HAMAs) before the treatment (Figure S5B). 1 month following the infusion, nearly complete eradication of tumor disease was observed (Figure 5I), accompanied by substantial expansion of CAR-T cells and notable inflammatory responses at the tumor site (Figures 5J and S5C–S5F). Unfortunately, the patient experienced a relapse 2 months after the treatment, with confirmed loss of CD19 expression (Figure S5G). However, CAR-T cells were still detectable in the breast lesion tissue through fluorescence-activated cell sorting (FACS) analysis, quantification of CAR-VCN (5,197.5 copies/μg), and next-generation sequencing (NGS) sequencing (Figures 5K and 5L). These findings, combined with the reappearance of CAR-T cells in patients with B cell recovery (Figure 5F), confirm that *SPPL3* deficiency enhances the survival capacity of allogeneic T cells in immune-recovered hosts.

TCR is critical for T cell persistence

Although *SPPL3*^{KO} CAR-T cells were detectable in tissues for up to 2 months and exhibited late expansion as CD3$^+$ CAR-T cells, their long-term persistence was not maintained. We hypothesized that the reduced persistence of infused allogeneic T cells might be attributed to TCR deletion, particularly given the significant expansion of CD3$^+$ CAR-T cells observed in patients (Figure 5F).

To directly examine the role of TCR in T cell longevity *in vivo* within a therapeutic transfer model, we carried out a syngeneic CD45.1$^+$ T cell transfer experiment. TCR-deleted T cells and control T cells were co-transferred into sub-lethally irradiated CD45.2$^+$ mice (Figures 6A and 6B). Over the subsequent weeks, we tracked the proportion of TCR-negative T cells and observed a gradual decline (Figures 6C and 6D), with a more pronounced reduction beginning 1 week post-transfer (Figures 6E and 6F). Notably, the percentages of TCR-negative T cells were significantly lower in the liver and bone marrow, suggesting tissue-specific differences that merit further investigation (Figure 6E).

These findings highlight the critical role of TCR in maintaining long-term T cell persistence. Based on clinical observations, reverse translational studies, and additional data,[9] we demonstrated that TCR signaling is indispensable for sustained CAR-T cell persistence and prolonged tumor control.

Alleviating GvHD through SPPL3 editing

Building on our discovery that SPPL3 deletion reduces TCR expression on T cells (Figure 3H), we hypothesize that targeting SPPL3 alone could mitigate GvHD risk without requiring TCR deletion.

To evaluate the impact of enhanced glycosylation on TCR-mediated functionality, we conducted experiments using human cytomegalovirus (HCMV) antigen-specific T cells. PBMCs from HLA-A2 donors were pulsed with the NLVPMVATV (NLV) peptide (pp65 495–503) and co-cultured with allogeneic CMV-specific T cells (Figure 6G). *SPPL3*^{KO} TCR-T cells exhibited reduced proliferation in response to HLA/peptide stimulation, indicating attenuated TCR-mediated activity (Figures 6H and 6I).

To further assess the GvHD activity of *SPPL3*^{KO} anti-CD19 CAR-T cells, we utilized a humanized mouse model (Figure 6J). Compared with mock T cells and conventional CAR-T cells, *SPPL3*^{KO} anti-CD19 CAR-T cells exhibited reduced proliferation and correspondingly lower GvHD scores (Figures 6K and 6L). Histological assessment also revealed less tissue damage in key organs—including the liver, spleen, and lungs—in mice treated with *SPPL3*^{KO} CAR-T cells versus controls (Figure S6A). Collectively, these results demonstrate that SPPL3 deletion dampens TCR-antigen interactions, leading to restrained—but not abolished—T cell proliferation, thereby markedly lowering the risk of GvHD.

Safety of TCR-sufficient SPPL3 ^{KO} anti-CD19 CAR-T cells in patients

Encouraged by initial cohort results—showing that *SPPL3*^{KO} T cells exhibit low GvHD risk, potent anti-tumor activity, prolonged persistence, and stable glycan-modified phenotypes *in vivo*—alongside supportive preclinical evidence of effective tumor control in mouse models (Figures S6B–S6D), we designed a second phase I clinical trial (NCT06323525). Following

(D) Best responses achieved by enrolled patients, categorized based on administered dose levels.
(E) Representative positron emission tomography (PET)-computed tomography (CT) scans at baseline, 1 month, and 3 months post CAR-T infusion. Visualization of tumor lesion disappearance (CR) in Pt 06 and Pt 20 following CAR-T infusion. Arrow in the panel of Pt 06 indicates the enlarged spleen (left).
(F) Expansion profiles of CD3$^-$CAR$^+$, CD3$^+$CAR$^+$, and B cells in peripheral blood over the course of therapy.
(G) PET-CT imaging of tumor lesions in Pt 11 pre-CAR-T therapy (left) and ultrasound images showing abdominal fluid accumulation on day 9 post-therapy (right). Plot of identification and analysis of CAR-T cells in the peritoneal cavity on day 9, with gating performed on live lymphocytes.
(H) Comparative detection of specific molecules on host T cells and CAR-T cells extracted from ascites.
(I) Visualization of tumor size changes in Pt 01 via PET-CT imaging, comparing baseline and 1-month post-CAR-T infusion.
(J) Longitudinal monitoring of CD3$^-$CAR$^+$, CD3$^+$CAR$^+$, and B cell expansion in peripheral blood.
(K) Detection of infused cells in breast lesion tissue 2 months post-CAR-T therapy using donor-specific anti-HLA antibodies.
(L) NGS analysis of edited cells extracted from the breast lesion tissue.
The data in (C) ($n = 9$) are reported as means ± SDs. Statistical analysis in (H) used a t test: $^*p < 0.05$, $^{**}p < 0.01$, $^{***}p < 0.001$.
See also Figures S3–S5 and Tables S1–S3.

Please cite this article in press as: Wu et al., Glycan shielding enables TCR-sufficient allogeneic CAR-T therapy, Cell (2025), https://doi.org/10.1016/j.cell.2025.07.046

CellPress
OPEN ACCESS

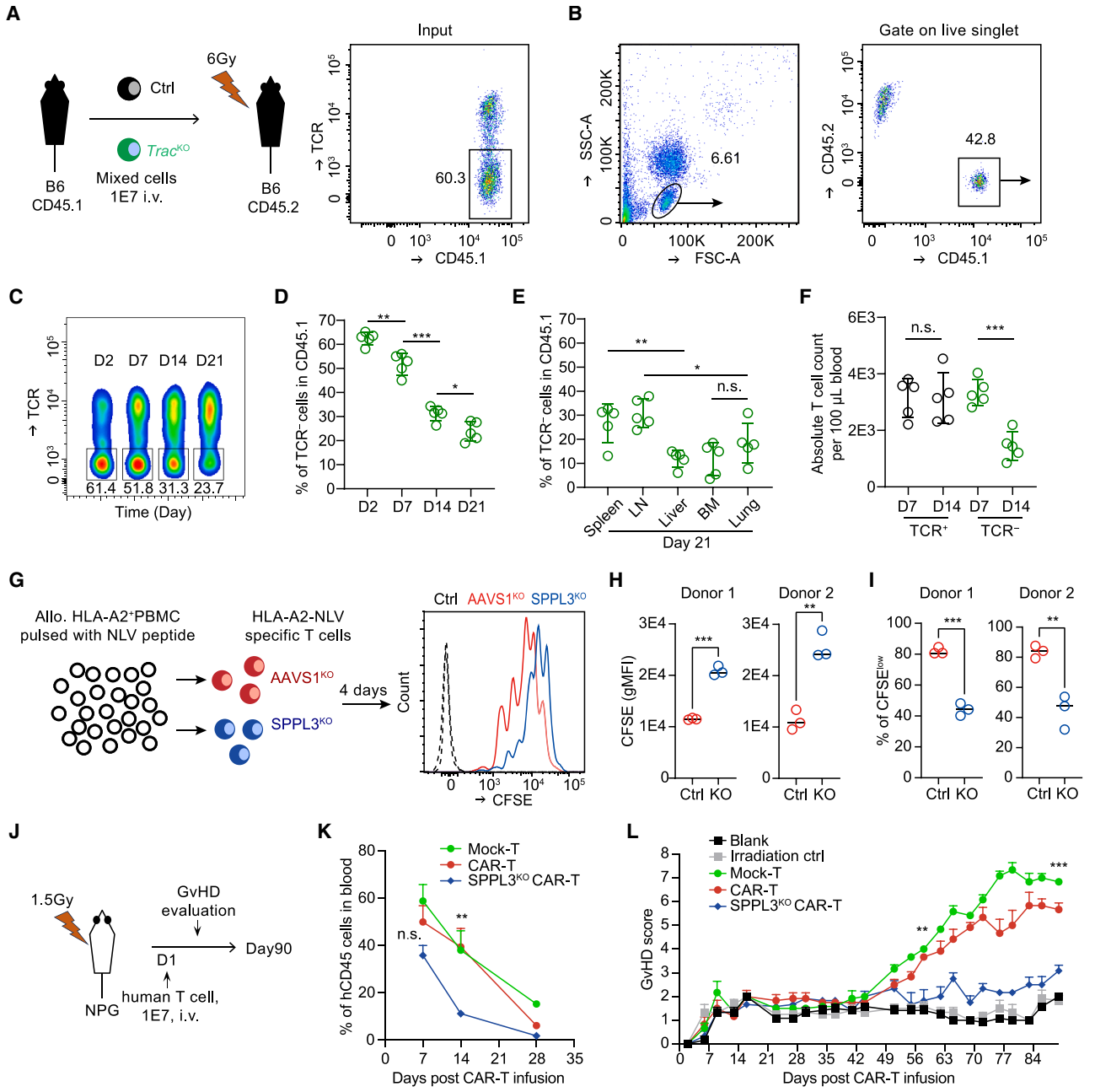

Figure 6. Tracking TCR-negative T cells *in vivo* and attenuated GvH reactions of *SPPL3*^{KO} T cells

(A) Schematic representation of the experimental setup.
(B) Gating strategy employed to identify transferred cells.
(C) Representative plots showing the percentage of TCR-negative T cells among transferred cells at various time points.
(D) Cumulative results displaying the percentage of TCR-negative T cells throughout the experiment.
(E) Percentage of TCR-negative T cells among transferred cells in different organs on day 21.
(F) Absolute counts of transferred T cells at days 7 and 14.
(G) Mixed culture of knockout cells (*SPPL3*^{KO} or *AAVS1*^{KO}) and peptide-pulsed PBMCs at a 1:10 ratio for 4 days.
(H and I) Analysis of the proliferation of HCMV-specific T cells from two donors. Dye dilutions were used to evaluate proliferation.
(J) Schematic representation of the experimental setup.
(K) Tracking the number of transferred cells at various time points throughout the experiment.
(L) Comparison of GvHD scores among different groups receiving human T cells. Horizontal lines indicate the mean.
The data presented in (D) ($n = 5$), (E) ($n = 5$), (F) ($n = 5$), (H) ($n = 3$), (I) ($n = 3$), (K) ($n = 6$), and (L) ($n = 6$) are shown as means ± SDs. Statistical analyses were performed using the Mann-Whitney U test for (D), (E), (I), and (K). Other panels were analyzed using a t test; $^{*}p < 0.05$, $^{**}p < 0.01$, $^{***}p < 0.001$.
See also Figure S6.

Please cite this article in press as: Wu et al., Glycan shielding enables TCR-sufficient allogeneic CAR-T therapy, Cell (2025), https://doi.org/10.1016/j.cell.2025.07.046

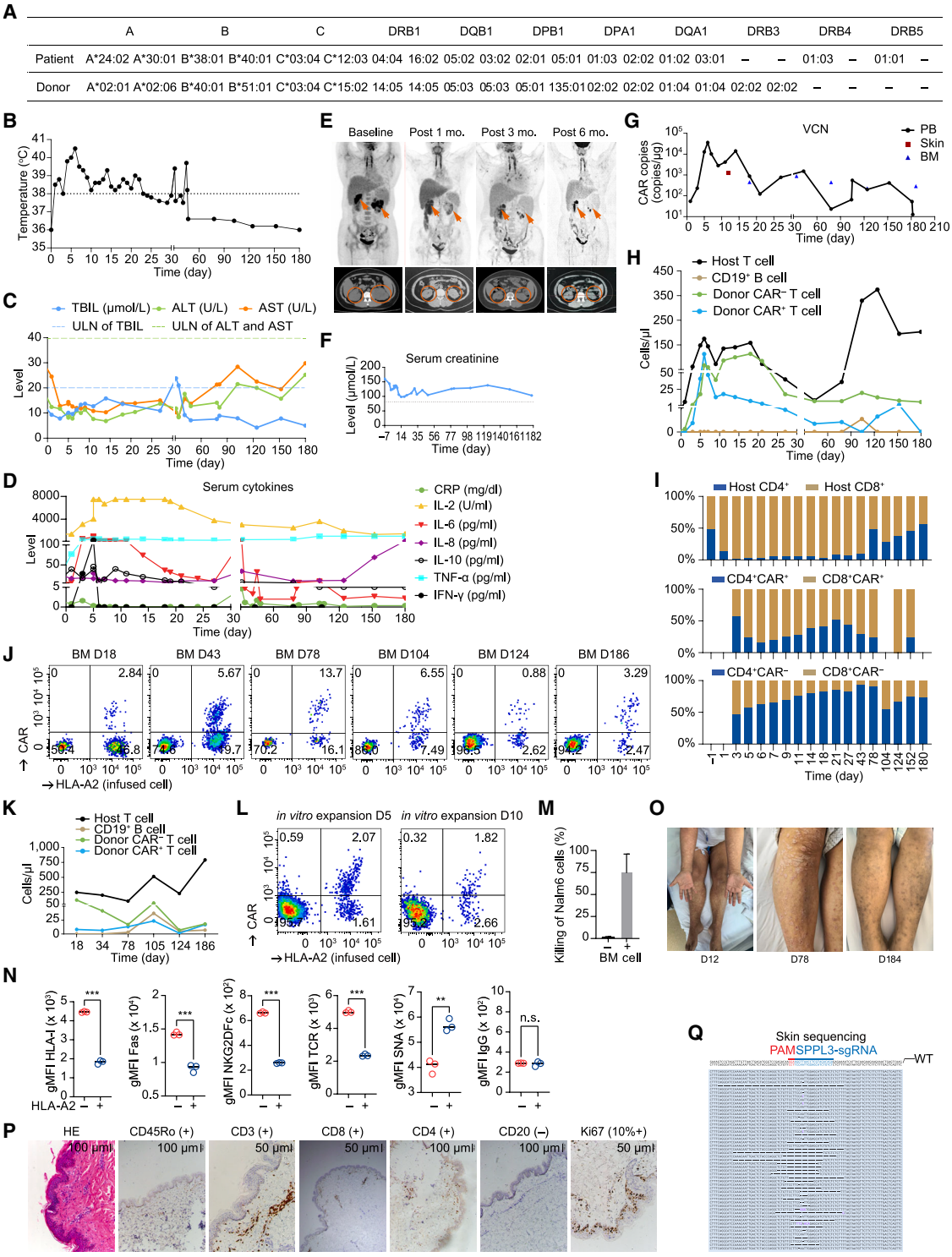

Figure 7. Long persistence of *SPPL3*^{KO}/anti-CD19 CAR-T cells *in vivo*

(A) HLA information of the donor and recipient.

(B) Patient's body temperature during CAR-T therapy.

(C) Liver function assessments at various time points.

(D) Serum cytokine concentrations during CAR-T therapy.

(E) PET-CT scans of pre-infusion at 1, 3, and 6 months post-CAR-T infusion.

(legend continued on next page)

Please cite this article in press as: Wu et al., Glycan shielding enables TCR-sufficient allogeneic CAR-T therapy, Cell (2025), https://doi.org/10.1016/j.cell.2025.07.046

lymphodepletion with fludarabine and cyclophosphamide, patients receive a single infusion of TCR-sufficient *SPPL3*^{KO}/anti-CD19 CAR-T cells at escalating doses using a 3 + 3 design. The primary endpoints are the assessment of DLTs within 28 days post-infusion and the evaluation of potential GvHD. The study is currently recruiting, and outcomes will be reported in due course. Here, we present the clinical course of three patients who received this CAR-T therapy on a compassionate care basis after failing to meet the formal eligibility criteria of this ongoing phase I trial (see STAR Methods for details). The study was approved by the institutional ethics committee, and all three patients provided written informed consent.

Patient C01

Patient C01, a 33-year-old female diagnosed with diffuse large B cell lymphoma, received compassionate-use therapy after third-line systemic chemotherapy. She was enrolled on April 17, 2024, and received the infusion on June 6, 2024. The donor and recipient shared a 3/12 HLA match, indicating an unrelated donor setting (Figure 7A). Post-infusion, the patient experienced a prolonged fever but maintained normal liver function (Figures 7B and 7C). Cytokine levels peaked during the first week and normalized, while interleukin-2 (IL-2) levels exceeded 100 U/mL in subsequent days (Figure 7D). The patient developed grade 1 CRS (lasting from 13 h post-infusion to day 14) and grade 2 ICANS (occurring on days 5 and 6) (Table S4). Both CRS and ICANS were resolved post treatment. Additional transient AEs included grade 2 head and neck edema (days 4–8), grade 1 diarrhea, and grade 1 coagulation abnormalities noted on day 5.

The patient achieved CR 1 month post-infusion, which was sustained at 3 and 6 months (Figure 7E). Despite pre-existing kidney lesions and elevated serum creatinine levels, improvements were noted following CAR-T therapy (Figure 7F). CAR-VCN levels were consistently detectable in peripheral blood, skin, and bone marrow (Figure 7G). The CAR$^+$ T cell count in peripheral blood peaked at 112.81 cells/μL on day 6 and successfully suppressed B cell recovery for up to 180 days (Figure 7H). Notably, CAR$^-$ donor T cells expanded alongside host T cells during the bone marrow suppressive phase (Figure 7H). Host T cells were predominantly CD8$^+$, while most donor CAR$^+$ cells were also CD8$^+$. By contrast, CAR$^-$ donor cells exhibited a higher proportion of CD4$^+$ cells (Figure 7I).

Although no lymphoma infiltration was detected in the bone marrow, CAR$^+$ T cells persisted for up to 6 months (Figure 7J). Bone marrow analyses showed B cell suppression, correlating with CAR-T cell dynamics to suggest ongoing tumor surveillance (Figure 7K). *In vitro* studies confirmed that CAR-T cells isolated from the bone marrow retained robust tumor-killing activity and could expand without immediate rejection by host T cells (Figures 7L and 7M). Notably, infused T cells exhibited reduced expression of HLA-I, Fas, crystallizable fragment engineered NKG2D-IgG fusion protein (NKG2D-Fc), and TCR, alongside enhanced Sambucus Nigra lectin (SNA) compared with host T cells (Figure 7N).

On day 8, the patient developed a grade 1–3 skin rash that spread from the limbs to the trunk, accompanied by itching but no pain (Figure 7O). A skin biopsy taken from the abdomen on day 12 revealed netted basket keratosis, mild epidermal thinning, increased basal pigmentation, focal vacuolar degeneration of the basal membrane, and infiltration of lymphocytes with eosinophils (Figure 7P). Despite these skin changes, histopathology at the peak of the rash showed no apoptotic activity or evidence of classical GvHD (Figure 7P). Donor T cells remained detectable in skin tissue on day 12, as confirmed by FACS analysis (host-to-donor ratio 2:1; CAR$^-$ to CAR$^+$ ratio 10:1), CAR-VCN quantification (1,212.12 copies/μg), and NGS analysis (Figure 7Q). By day 77, the patient had no systemic, hepatic, or gastrointestinal symptoms. The rash presented as peeling, thickened, and hardened skin with associated itching. GvHD-associated markers remained comparable to baseline during both the early (day 11) and late (day 77) stages of the rash, except for increased elafin levels at day 77, indicating a low risk of GvHD (Figure S7A). The rash resolved spontaneously by day 124 without immunosuppressive treatment, leaving only post-inflammatory hyperpigmentation (Figure 7O). The patient developed eosinophilia by day 18 post-infusion, coinciding with the presence of donor T cells in the bone marrow (Figure S7B), while the exact mechanism remains unclear.

Patient C02

Patient C02, a 27-year-old woman diagnosed with primary mediastinal large B cell lymphoma, received compassionate-use treatment. The patient was ineligible for trial enrollment due to left lung atelectasis and type I respiratory failure from tumor compression. The patient was enrolled on February 13, 2025, and received the infusion on February 24, 2025. HLA compatibility with the unrelated donor was 2/12 (Figure S7C).

After infusion, the patient developed grade 2 CRS (days 1–14) without ICANS (Table S4). Transient grade 1 elevations in alanine

(F) Serum creatinine levels during CAR-T therapy.
(G) Quantification of CAR copies in peripheral blood, skin, and bone marrow.
(H) Monitoring the expansion of host T cells, donor T cells, and B cells in peripheral blood over time.
(I) CD4 and CD8 positive cell percentages in host T cells and donor T cells in peripheral blood.
(J) Infused T cell detection in bone marrow at different time points.
(K) Tracking the host T cells, donor T cells, and B cells in bone marrow over time.
(L) Expansion of CAR-T cells from bone marrow obtained at day 124.
(M) Evaluation of target cell killing using bone marrow cells containing CAR-T cells.
(N) Comparative analysis of specified molecules on host T cells and HLA-A2$^+$ donor cells in bone marrow.
(O) Skin manifestations at various time intervals.
(P) Histological examination of the skin sample on day 12.
(Q) NGS analysis of edited cells isolated from the skin. Horizontal lines represent the mean. Statistical analysis was performed using the t test in (N); $^{**}p < 0.01$, $^{***}p < 0.001$.
See also Figure S7 and Table S4.

Please cite this article in press as: Wu et al., Glycan shielding enables TCR-sufficient allogeneic CAR-T therapy, Cell (2025), https://doi.org/10.1016/j.cell.2025.07.046

aminotransferase (ALT), aspartate aminotransferase (AST), and bilirubin occurred on day 21 (Table S4). A grade 1 rash emerged on days 27–30, which resolved with halometasone ointment and tacrolimus ointment. The patient did not develop diarrhea, and there was no evidence of acute GvHD. IL-2 levels remained elevated for more than a month (Figure S7D).

At 1 month, the patient achieved a PR (Figure S7E). Peak CAR-VCN reached 314,146.34 copies/μg (day 9) (Figure S7F), and CAR^+ T cell levels peaked at 313.3 cells/μL (day 7). Bone marrow analysis (day 21) confirmed CAR^+ and CAR^- T cell levels comparable to those in peripheral blood (Figure S7G). A higher expansion of donor T cells was observed in Pt C02 compared with Pt C01, which may be related to a higher tumor burden.

Patient C03

Patient C03, a 34-year-old male with high-risk mixed lineage leukemia (MLL)-rearranged B cell acute lymphoblastic leukemia (B-ALL), was diagnosed in August 2023 with an initial marrow blast count of 76.82%. The patient was ineligible for trial enrollment due to uncontrolled fungal pneumonia and a bacterial lower limb infection identified during screening and was therefore treated under compassionate use. The patient was enrolled on January 7, 2025, and received the infusion on February 20, 2025. He then received *SPPL3*^{KO} CAR-T cells from a fully HLA-mismatched (0/12) unrelated donor (Figure S7H). Post-infusion, the patient experienced grade 1 CRS (days 1–8) and grade 1 ICANS (day 6), managed with 300 mg infliximab (day 3). A transient grade 2 diarrhea episode occurred on day 6, with no liver or skin involvement and no signs of acute GvHD (Table S4). Cytokine levels peaked within the first week (Figure S7I).

Remarkably, the patient achieved minimal residual disease (MRD)-negative complete remission with incomplete count recovery (CRi) by days 14 and 28 (Figure S7J). Peak CAR-VCN was 90,881.46 copies/μg (day 7), with CAR^+ T cell levels at 23.02 cells/μL on the same day in peripheral blood (Figures S7K and S7L). B cells remained undetectable throughout the monitoring period (Figure S7L). These findings further support the clinical potential of *SPPL3*^{KO}/anti-CD19 CAR-T cells as a therapeutic option for heavily pretreated or refractory malignancies.

DISCUSSION

Together, these data provide several key findings. First, we identified *SPPL3* as a prominent gene target for promoting the persistence of allogeneic T cells. Masking universal T cells with glycans regulated by SPPL3 protects them from cellular and soluble immune effectors and results in an early high expansion of these cells in humans. The complete extent and specificity of SPPL3's impact on proteins and ceramide glycans remain elusive. It also remains uncertain whether SPPL3 selectively shapes immune resistance-related molecules from an evolutionary standpoint. Supporting this notion, clinical DNA sequencing data reveal a naturally occurring SPPL3 mutation associated with a low level of T cell infiltration, suggesting a potential connection.[43]

Our reverse translational study underscores the critical role of TCR in promoting T cell persistence, especially in universal CAR-T cells where the TCR complex is intentionally disrupted to mitigate GvHD. These findings align with our previous research, which demonstrated that TCR^+ CAR-T cells exhibited significantly greater expansion compared with their TCR^- counterparts.[50] Although the mechanisms driving this persistence advantage remain unclear, one possibility is that tonic signaling mediated by the TCR provides a survival benefit to T cells.[51,52]

Applying allogeneic anti-CD19 CAR-T cells in tumor patients poses greater challenges than in autoimmune diseases, largely because of the critical need for long-term persistence in the former. To enhance the durability of allogeneic T cells, adopting a TCR-sufficient universal T cell strategy is crucial.

In the context of *SPPL3*^{KO} anti-CD19 CAR-T cell therapy, no definitive evidence of >grade II GvHD was observed. Histological, immunological, clinical, and temporal evidence strongly suggests that the observed rash does not represent GvHD but rather aligns more closely with a self-limiting, non-destructive inflammatory response. We observed reciprocal allogeneic reactions between donor-derived and host-derived T cells. Supported by extensive experimental and clinical evidence, we propose defining this phenomenon as bidirectional allogeneic T cell reaction syndrome (BATCRS). BATCRS describes an immune state characterized by simultaneous, mild, mutual interactions between donor and recipient T cells in an allogeneic environment, such as transplantation or *SPPL3*^{KO} CAR-T therapy (see STAR Methods for details).

Our work has showcased the successful expansion and sustained presence of *SPPL3*^{KO}/anti-CD19 CAR-T cells in patients with r/r B-NHL, resulting in effective tumor control. The combination of >98.5% SPPL3 knockout efficiency, expected phenotypic alterations in CAR-T cells, and detection of edited cells in tumor lesions demonstrates both successful genome editing and biologically relevant *in vivo* persistence. Overall, these findings contribute insights into glycan-shielded CAR-T cells as a potential universal therapeutic approach, with implications for transplantation and the development of therapeutics.

Limitations of the study

Our study supports glycan-shielded CAR-T cells as a universal therapeutic approach. Although the study demonstrated the significant contribution of *SPPL3*^{KO} CAR-T cells to positive patient outcomes and long persistence in patients, further evaluation in cohorts of patients is needed. The relatively higher incidence of CRS observed in our cohort can likely be attributed to factors such as increased tumor burden, robust CAR-T cell expansion, and BATCRS responses in the allogeneic setting. This underscores the importance of rigorous monitoring and evaluation of cytokine-associated toxicities in future cohorts. Furthermore, a comprehensive assessment of GvHD remains crucial, particularly given the potential presence of rare high-affinity TCR clones that could target host cells in heterogeneous HLA backgrounds. *SPPL3*^{KO} CAR-T cells partially reduce the detection of HLA and TCR molecules, but some level of interaction promoting endogenous immunity is inevitable. These interactions may enhance the graft-versus-tumor effect of host T cells through mechanisms such as IL-2 availability or alloantigen priming. Finally, extending this approach to solid tumors warrants additional investigation to evaluate its safety and efficacy in these more challenging contexts.

RESOURCE AVAILABILITY

Lead contact

Further information and requests for resources and reagents should be directed to and will be fulfilled by the lead contact, Wensheng Wei (wswei@pku.edu.cn).

Materials availability

Plasmids and other reagents generated in this study are available from the lead contact upon reasonable request.

Data and code availability

- The raw LC-MS files supporting the findings of this study have been deposited to the ProteomeXchange Consortium via the PRIDE partner repository with the dataset identifier PRIDE: PXD052748 (https://www.proteomexchange.org/).
- RNA-seq data are accessible through the NGDC Sequence Archive database with accession code NGDC: PRJCA040498.

ACKNOWLEDGMENTS

We thank Changping Laboratory for their support. We thank members of the Wei laboratory and Han laboratory for comments and experimental assistance. We thank Ms. Bei Wang for soft infrastructure assistance. We thank Dr. Ying Yu for technical assistance. W.H. received funding from the National Science Foundation of China (NSFC) (82341208 and 82430012) and the Noncommunicable Chronic Diseases-National Science and Technology Major Project (2023ZD0501300). W.W. received funding from the NSFC (82341207), the Noncommunicable Chronic Diseases-National Science and Technology Major Project (2024ZD0537704), the Peking-Tsinghua Center for Life Sciences, and Changping Laboratory. Zeguang Wu received funding from the State Key Laboratory for Diagnosis and Treatment of Severe Zoonotic Infectious Diseases (2024KF00001), the NSFC (82350119), and the National Key Research and Development Program of China (2023YFC2308600). C.C. L.W. received funding from the NSFC (32150005), the Ministry of Science and Technology of China (2022YFA0806000), the Clinical Research Operating Fund of Central High-level Hospitals (2022-PUMCH-E-001), the Medical and Scientific Innovation Project of the Chinese Academy of Medical Science (2022-12M-1-004), and the Talent Program of the Chinese Academy of Medical Science (2022-RC310-10). J.S. received funding from the NSFC (82202988). C.C. received funding from the CAMS Innovation Fund for Medical Sciences (2024-I2M-3-001).

AUTHOR CONTRIBUTIONS

Zeguang Wu, W.H., and W.W. conceived the project, designed the experiments, performed the research, analyzed data, and wrote the manuscript. Zeguang Wu, Q.L., Y.Q., J.Y., X.S., H.Z., Z.Y., Yunyi Zhang, Y.Y., X.Z., Y.S., K.M., L. Yu, H.Y., Z. Wang, W.Z., Z.Z., L. Yang, and M.J. performed research and analyzed data. J.S., Y.L., Q.Y., C.W., Z.L., Zhiqiang Wu, Y.W., and W.H. designed the clinical trial, performed the research, and analyzed clinical data. J.S. wrote the manuscript. W.T., C.C., and Yongjian Zhang performed the bioinformatics analyses. Zeguang Wu, F.L., C.C.L.W., P.Y., W.H., and W.W. supervised the project. All authors discussed the results and contributed to the final manuscript.

DECLARATION OF INTERESTS

A patent application has been filed by Peking University (with W.W., Zeguang Wu, Q.L., J.Y., and Y.Q. as inventors). F.L., H.Z., Z.Y., Yunyi Zhang, Y.Y., X.Z., Y.S., L. Yang, Yongjian Zhang, M.J., and P.Y. are employees of EdiGene Inc. W.W. is a founder and scientific adviser for EdiGene and Therorna Inc.

STAR★METHODS

Detailed methods are provided in the online version of this paper and include the following:

- KEY RESOURCES TABLE
- EXPERIMENTAL MODEL AND STUDY PARTICIPANT DETAILS
  - Clinical trials design
  - Extended clinical details for SPPL3^{KO}/TCR^{KO} CAR-T cell therapy
  - Extended clinical details for SPPL3^{KO} CAR-T cell therapy
  - Animals
  - Cell lines
  - Primary cells
- METHOD DETAILS
  - Assessment of response
  - Assessment and grading of CRS
  - Assessment and grading of ICANS
  - Assessment and grading of GvHD
  - Assessment and grading of adverse events (AEs)
  - Bidirectional Allogeneic T-Cell Reaction Syndrome (BATCRS)
  - Cytotoxicity assessment
  - Generation of engineered T-cells
  - Lentiviral production and infection
  - Indel analysis
  - Genome-wide CRISPR screen, functional enrichment analysis
  - Flow cytometry based competitive killing assay
  - RNA-seq analysis
  - Immunohistochemistry
  - Cellular membrane fraction and Western Blot
  - LC-MS/MS analysis for the differentially expressed proteins
  - Immunoprecipitation
  - Proteolytic glycopeptides preparation
  - LC-MS/MS analysis for glycans
  - Database search and glycans analysis
- QUANTIFICATION AND STATISTICAL ANALYSIS
- ADDITIONAL RESOURCES

SUPPLEMENTAL INFORMATION

Supplemental information can be found online at https://doi.org/10.1016/j.cell.2025.07.046.

Received: June 26, 2024
Revised: April 25, 2025
Accepted: July 30, 2025

REFERENCES

1. June, C.H., and Sadelain, M. (2018). Chimeric Antigen Receptor Therapy. N. Engl. J. Med. *379*, 64–73. https://doi.org/10.1056/NEJMra1706169.
2. Finck, A.V., Blanchard, T., Roselle, C.P., Golinelli, G., and June, C.H. (2022). Engineered cellular immunotherapies in cancer and beyond. Nat. Med. *28*, 678–689. https://doi.org/10.1038/s41591-022-01765-8.
3. Zhang, Y., Wang, Y., Liu, Y., Tong, C., Wang, C., Guo, Y., Ti, D., Yang, Q., Qiao, S., Wu, Z., et al. (2022). Long-term activity of tandem CD19/CD20 CAR therapy in refractory/relapsed B-cell lymphoma: a single-arm, phase 1–2 trial. Leukemia *36*, 189–196. https://doi.org/10.1038/s41375-021-01345-8.
4. Dai, H., Wu, Z., Jia, H., Tong, C., Guo, Y., Ti, D., Han, X., Liu, Y., Zhang, W., Wang, C., et al. (2020). Bispecific CAR-T cells targeting both CD19 and CD22 for therapy of adults with relapsed or refractory B cell acute lymphoblastic leukemia. J. Hematol. Oncol. *13*, 30. https://doi.org/10.1186/s13045-020-00856-8.

5. Labanieh, L., and Mackall, C.L. (2023). CAR immune cells: design principles, resistance and the next generation. Nature *614*, 635–648. https://doi.org/10.1038/s41586-023-05707-3.

6. Chen, S., and van den Brink, M.R.M. (2024). Allogeneic "Off-the-Shelf" CAR T cells: Challenges and advances. Best Pract. Res. Clin. Haematol. *37*, 101566. https://doi.org/10.1016/j.beha.2024.101566.

7. Hu, X., Manner, K., DeJesus, R., White, K., Gattis, C., Ngo, P., Bandoro, C., Tham, E., Chu, E.Y., Young, C., et al. (2023). Hypoimmune anti-CD19 chimeric antigen receptor T cells provide lasting tumor control in fully immunocompetent allogeneic humanized mice. Nat. Commun. *14*, 2020. https://doi.org/10.1038/s41467-023-37785-2.

8. Wang, X., Wu, X., Tan, B., Zhu, L., Zhang, Y., Lin, L., Xiao, Y., Sun, A., Wan, X., Liu, S., et al. (2024). Allogeneic CD19-targeted CAR-T therapy in patients with severe myositis and systemic sclerosis. Cell *187*, 4890–4904. e9. https://doi.org/10.1016/j.cell.2024.06.027.

9. Qasim, W., Zhan, H., Samarasinghe, S., Adams, S., Amrolia, P., Stafford, S., Butler, K., Rivat, C., Wright, G., Somana, K., et al. (2017). Molecular remission of infant B-ALL after infusion of universal TALEN gene-edited CAR T cells. Sci. Transl. Med. *9*, eaaj2013. https://doi.org/10.1126/scitranslmed.aaj2013.

10. Menegatti, S., Lopez-Cobo, S., Sutra Del Galy, A., Fuentealba, J., Silva, L., Perrin, L., Heurtebise-Chrétien, S., Pottez-Jouatte, V., Darbois, A., Burgdorf, N., et al. (2024). Ablation of FAS confers allogeneic $CD3^-$ CAR T cells with resistance to rejection by T cells and natural killer cells. Nat. Biomed. Eng. *8*, 1651–1664. https://doi.org/10.1038/s41551-024-01282-8.

11. Tschumi, B.O., Dumauthioz, N., Marti, B., Zhang, L., Lanitis, E., Irving, M., Schneider, P., Mach, J.P., Coukos, G., Romero, P., et al. (2018). CART cells are prone to Fas- and DR5-mediated cell death. J. Immunother. Cancer *6*, 71. https://doi.org/10.1186/s40425-018-0385-z.

12. Künkele, A., Johnson, A.J., Rolczynski, L.S., Chang, C.A., Hoglund, V., Kelly-Spratt, K.S., and Jensen, M.C. (2015). Functional Tuning of CARs Reveals Signaling Threshold above Which CD8+ CTL Antitumor Potency Is Attenuated due to Cell Fas-FasL-Dependent AICD. Cancer Immunol. Res. *3*, 368–379. https://doi.org/10.1158/2326-6066.CIR-14-0200.

13. McKenzie, C., El-Kholy, M., Parekh, F., Robson, M., Lamb, K., Allen, C., Sillibourne, J., Cordoba, S., Thomas, S., and Pule, M. (2023). Novel Fas-TNFR chimeras that prevent Fas ligand-mediated kill and signal synergistically to enhance CAR T cell efficacy. Mol. Ther. Nucleic Acids *32*, 603–621. https://doi.org/10.1016/j.omtn.2023.04.017.

14. Perica, K., Kotchetkov, I.S., Mansilla-Soto, J., Ehrich, F., Herrera, K., Shi, Y., Dobrin, A., Gönen, M., and Sadelain, M. (2025). HIV immune evasin Nef enhances allogeneic CAR T cell potency. Nature *640*, 793–801. https://doi.org/10.1038/s41586-025-08657-0.

15. Guo, Y., Tong, C., Su, L., Zhang, W., Jia, H., Liu, Y., Yang, Q., Wu, Z., Wang, Y., and Han, W. (2022). CRISPR/Cas9 genome-edited universal CAR T cells in patients with relapsed/refractory lymphoma. Blood Adv. *6*, 2695–2699. https://doi.org/10.1182/bloodadvances.2021006232.

16. Benjamin, R., Graham, C., Yallop, D., Jozwik, A., Mirci-Danicar, O.C., Lucchini, G., Pinner, D., Jain, N., Kantarjian, H., Boissel, N., et al. (2020). Genome-edited, donor-derived allogeneic anti-CD19 chimeric antigen receptor T cells in paediatric and adult B-cell acute lymphoblastic leukaemia: results of two phase 1 studies. Lancet *396*, 1885–1894. https://doi.org/10.1016/S0140-6736(20)32334-5.

17. Chiesa, R., Georgiadis, C., Syed, F., Zhan, H., Etuk, A., Gkazi, S.A., Preece, R., Ottaviano, G., Braybrook, T., Chu, J., et al. (2023). Base-Edited CAR7 T Cells for Relapsed T-Cell Acute Lymphoblastic Leukemia. N. Engl. J. Med. *389*, 899–910. https://doi.org/10.1056/NEJMoa2300709.

18. Jo, S., Das, S., Williams, A., Chretien, A.S., Pagliardini, T., Le Roy, A., Fernandez, J.P., Le Clerre, D., Jahangiri, B., Chion-Sotinel, I., et al. (2022). Endowing universal CAR T-cell with immune-evasive properties using TALEN-gene editing. Nat. Commun. *13*, 3453. https://doi.org/10.1038/s41467-022-30896-2.

19. Hu, Y., Zhou, Y., Zhang, M., Zhao, H., Wei, G., Ge, W., Cui, Q., Mu, Q., Chen, G., Han, L., et al. (2022). Genetically modified CD7-targeting allogeneic CAR-T cell therapy with enhanced efficacy for relapsed/refractory CD7-positive hematological malignancies: a phase I clinical study. Cell Res. *32*, 995–1007. https://doi.org/10.1038/s41422-022-00721-y.

20. Bix, M., Liao, N.S., Zijlstra, M., Loring, J., Jaenisch, R., and Raulet, D. (1991). Rejection of class I MHC-deficient haemopoietic cells by irradiated MHC-matched mice. Nature *349*, 329–331. https://doi.org/10.1038/349329a0.

21. Joncker, N.T., Fernandez, N.C., Treiner, E., Vivier, E., and Raulet, D.H. (2009). NK cell responsiveness is tuned commensurate with the number of inhibitory receptors for self-MHC class I: the rheostat model. J. Immunol. *182*, 4572–4580. https://doi.org/10.4049/jimmunol.0803900.

22. Ludigs, K., Jandus, C., Utzschneider, D.T., Staehli, F., Bessoles, S., Dang, A.T., Rota, G., Castro, W., Zehn, D., Vivier, E., et al. (2016). NLRC5 shields T lymphocytes from NK-cell-mediated elimination under inflammatory conditions. Nat. Commun. *7*, 10554. https://doi.org/10.1038/ncomms10554.

23. Li, G., Li, X., Zhuang, S., Wang, L., Zhu, Y., Chen, Y., Sun, W., Wu, Z., Zhou, Z., Chen, J., et al. (2022). Gene editing and its applications in biomedicine. Sci. China Life Sci. *65*, 660–700. https://doi.org/10.1007/s11427-021-2057-0.

24. Jongsma, M.L.M., de Waard, A.A., Raaben, M., Zhang, T., Cabukusta, B., Platzer, R., Blomen, V.A., Xagara, A., Verkerk, T., Bliss, S., et al. (2021). The SPPL3-defined glycosphingolipid repertoire orchestrates HLA class I-mediated immune responses. Immunity *54*, 387. https://doi.org/10.1016/j.immuni.2021.01.016.

25. Zhuang, X., Woods, J., Ji, Y., Scheich, S., Mo, F., Rajagopalan, S., Coulibaly, Z.A., Voss, M., Urlaub, H., Staudt, L.M., et al. (2024). Functional genomics identifies N-acetyllactosamine extension of complex N-glycans as a mechanism to evade lysis by natural killer cells. Cell Rep. *43*, 114105. https://doi.org/10.1016/j.celrep.2024.114105.

26. Verkerk, T., de Waard, A.A., Koomen, S.J.I., Sanders, J., Jorritsma, T., Pappot, A.T., Zandhuis, N.D., Zhang, T., Wuhrer, M., Hoogendijk, A.J., et al. (2025). Tumor-Expressed SPPL3 Supports Innate Antitumor Immune Responses. Eur. J. Immunol. *55*, e202451129. https://doi.org/10.1002/eji.202451129.

27. Liu, Y., Liu, Y., Niu, X., Chen, A., Li, Y., Yu, Y., Mo, B., Liu, Z., Xu, T., Cheng, J., et al. (2025). Massively parallel interrogation of human functional variants modulating cancer immunosurveillance. Signal Transduct. Target. Ther. *10*, 88. https://doi.org/10.1038/s41392-025-02171-5.

28. Wei, J., Long, L., Zheng, W., Dhungana, Y., Lim, S.A., Guy, C., Wang, Y., Wang, Y.D., Qian, C., Xu, B., et al. (2019). Targeting REGNASE-1 programs long-lived effector T cells for cancer therapy. Nature *576*, 471–476. https://doi.org/10.1038/s41586-019-1821-z.

29. Freitas, K.A., Belk, J.A., Sotillo, E., Quinn, P.J., Ramello, M.C., Malipatlolla, M., Daniel, B., Sandor, K., Klysz, D., Bjelajac, J., et al. (2022). Enhanced T cell effector activity by targeting the Mediator kinase module. Science *378*, eabn5647. https://doi.org/10.1126/science.abn5647.

30. Carnevale, J., Shifrut, E., Kale, N., Nyberg, W.A., Blaeschke, F., Chen, Y.Y., Li, Z., Bapat, S.P., Diolaiti, M.E., O'Leary, P., et al. (2022). RASA2 ablation in T cells boosts antigen sensitivity and long-term function. Nature *609*, 174–182. https://doi.org/10.1038/s41586-022-05126-w.

31. Kilian, M., Friedrich, M.J., Lu, K.H.N., Vonhören, D., Jansky, S., Michel, J., Keib, A., Stange, S., Hackert, N., Kehl, N., et al. (2024). The immunoglobulin superfamily ligand B7H6 subjects T cell responses to NK cell surveillance. Sci. Immunol. *9*, eadj7970. https://doi.org/10.1126/sciimmunol.adj7970.

32. Yi, F., Cohen, T., Zimmerman, N., Dündar, F., Zumbo, P., Eltilib, R., Brophy, E.J., Arkin, H., Feucht, J., Gormally, M.V., et al. (2024). CAR-engineered lymphocyte persistence is governed by a FAS ligand/FAS autoregulatory circuit. Preprint at bioRxiv. https://doi.org/10.1101/2024.02.26.582108.

33. Zhou, Y., Zhu, S., Cai, C., Yuan, P., Li, C., Huang, Y., and Wei, W. (2014). High-throughput screening of a CRISPR/Cas9 library for functional genomics in human cells. Nature *509*, 487–491. https://doi.org/10.1038/nature13166.

34. Zhu, S., Cao, Z., Liu, Z., He, Y., Wang, Y., Yuan, P., Li, W., Tian, F., Bao, Y., and Wei, W. (2019). Guide RNAs with embedded barcodes boost CRISPR-pooled screens. Genome Biol. *20*, 20. https://doi.org/10.1186/s13059-019-1628-0.

35. Peng, J., Zhou, Y., Zhu, S., and Wei, W. (2015). High-throughput screens in mammalian cells using the CRISPR-Cas9 system. FEBS Journal *282*, 2089–2096. https://doi.org/10.1111/febs.13251.

36. Sen, C.K., Sashwati, R., and Packer, L. (1999). Fas mediated apoptosis of human Jurkat T-cells: intracellular events and potentiation by redox-active alpha-lipoic acid. Cell Death Differ. *6*, 481–491. https://doi.org/10.1038/sj.cdd.4400514.

37. Voss, M., Künzel, U., Higel, F., Kuhn, P.H., Colombo, A., Fukumori, A., Haug-Kröper, M., Klier, B., Grammer, G., Seidl, A., et al. (2014). Shedding of glycan-modifying enzymes by signal peptide peptidase-like 3 (SPPL3) regulates cellular N-glycosylation. EMBO J. *33*, 2890–2905. https://doi.org/10.15252/embj.201488375.

38. Mentrup, T., Cabrera-Cabrera, F., Fluhrer, R., and Schröder, B. (2020). Physiological functions of SPP/SPPL intramembrane proteases. Cell. Mol. Life Sci. *77*, 2959–2979. https://doi.org/10.1007/s00018-020-03470-6.

39. Hirata, T., Takata, M., Tokoro, Y., Nakano, M., and Kizuka, Y. (2022). Shedding of N-acetylglucosaminyltransferase-V is regulated by maturity of cellular N-glycan. Commun. Biol. *5*, 743. https://doi.org/10.1038/s42003-022-03697-y.

40. Heard, A., Landmann, J.H., Hansen, A.R., Papadopolou, A., Hsu, Y.S., Selli, M.E., Warrington, J.M., Lattin, J., Chang, J., Ha, H., et al. (2022). Antigen glycosylation regulates efficacy of CAR T cells targeting CD19. Nat. Commun. *13*, 3367. https://doi.org/10.1038/s41467-022-31035-7.

41. Yan, X., Chen, D., Wang, Y., Guo, Y., Tong, C., Wei, J., Zhang, Y., Wu, Z., and Han, W. (2022). Identification of NOXA as a pivotal regulator of resistance to CAR T-cell therapy in B-cell malignancies. Signal Transduct. Target. Ther. *7*, 98. https://doi.org/10.1038/s41392-022-00915-1.

42. Kawaguchi, K., Yamamoto-Hino, M., and Goto, S. (2021). SPPL3-dependent downregulation of the synthesis of (neo)lacto-series glycosphingolipid is required for the staining of cell surface CD59. Biochem. Biophys. Res. Commun. *571*, 81–87. https://doi.org/10.1016/j.bbrc.2021.06.093.

43. Bentham, R., Litchfield, K., Watkins, T.B.K., Lim, E.L., Rosenthal, R., Martínez-Ruiz, C., Hiley, C.T., Bakir, M.A., Salgado, R., Moore, D.A., et al. (2021). Using DNA sequencing data to quantify T cell fraction and therapy response. Nature *597*, 555–560. https://doi.org/10.1038/s41586-021-03894-5.

44. Wu, Z., Park, S., Lau, C.M., Zhong, Y., Sheppard, S., Sun, J.C., Das, J., Altan-Bonnet, G., and Hsu, K.C. (2021). Dynamic variability in SHP-1 abundance determines natural killer cell responsiveness. Sci. Signal. *14*, eabe5380. https://doi.org/10.1126/scisignal.abe5380.

45. Sánchez-Martínez, D., Azaceta, G., Muntasell, A., Aguiló, N., Núñez, D., Gálvez, E.M., Naval, J., Anel, A., Palomera, L., Vilches, C., et al. (2015). Human NK cells activated by EBV$^+$ lymphoblastoid cells overcome anti-apoptotic mechanisms of drug resistance in haematological cancer cells. Oncoimmunology *4*, e991613. https://doi.org/10.4161/2162402X.2014.991613.

46. Nielsen, N., Ødum, N., Ursø, B., Lanier, L.L., and Spee, P. (2012). Cytotoxicity of CD56(bright) NK cells towards autologous activated CD4+ T cells is mediated through NKG2D, LFA-1 and TRAIL and dampened via CD94/NKG2A. PLoS One *7*, e31959. https://doi.org/10.1371/journal.pone.0031959.

47. Hammer, Q., Perica, K., Mbofung, R.M., van Ooijen, H., Martin, K.E., Momayyezi, P., Varady, E., Pan, Y., Jelcic, M., Groff, B., et al. (2024). Genetic ablation of adhesion ligands mitigates rejection of allogeneic cellular immunotherapies. Cell Stem Cell *31*, 1376–1386.e8. https://doi.org/10.1016/j.stem.2024.06.011.

48. Joung, J., Kirchgatterer, P.C., Singh, A., Cho, J.H., Nety, S.P., Larson, R.C., Macrae, R.K., Deasy, R., Tseng, Y.Y., Maus, M.V., et al. (2022). CRISPR activation screen identifies BCL-2 proteins and B3GNT2 as drivers of cancer resistance to T cell-mediated cytotoxicity. Nat. Commun. *13*, 1606. https://doi.org/10.1038/s41467-022-29205-8.

49. Varki, A. (2008). Sialic acids in human health and disease. Trends Mol. Med. *14*, 351–360. https://doi.org/10.1016/j.molmed.2008.06.002.

50. Wang, Z., Li, N., Feng, K., Chen, M., Zhang, Y., Liu, Y., Yang, Q., Nie, J., Tang, N., Zhang, X., et al. (2021). Phase I study of CAR-T cells with PD-1 and TCR disruption in mesothelin-positive solid tumors. Cell. Mol. Immunol. *18*, 2188–2198. https://doi.org/10.1038/s41423-021-00749-x.

51. Labrecque, N., Whitfield, L.S., Obst, R., Waltzinger, C., Benoist, C., and Mathis, D. (2001). How much TCR does a T cell need? Immunity *15*, 71–82. https://doi.org/10.1016/s1074-7613(01)00170-4.

52. Gascoigne, N.R.J., Rybakin, V., Acuto, O., and Brzostek, J. (2016). TCR Signal Strength and T Cell Development. Annu. Rev. Cell Dev. Biol. *32*, 327–348. https://doi.org/10.1146/annurev-cellbio-111315-125324.

53. Cooke, K.R., Kobzik, L., Martin, T.R., Brewer, J., Delmonte, J., Jr., Crawford, J.M., and Ferrara, J.L. (1996). An experimental model of idiopathic pneumonia syndrome after bone marrow transplantation: I. The roles of minor H antigens and endotoxin. Blood *88*, 3230–3239. https://doi.org/10.1182/blood.V88.8.3230.bloodjournal8883230.

54. Lee, D.W., Santomasso, B.D., Locke, F.L., Ghobadi, A., Turtle, C.J., Brudno, J.N., Maus, M.V., Park, J.H., Mead, E., Pavletic, S., et al. (2019). ASTCT Consensus Grading for Cytokine Release Syndrome and Neurologic Toxicity Associated with Immune Effector Cells. Biol. Blood Marrow Transplant. *25*, 625–638. https://doi.org/10.1016/j.bbmt.2018.12.758.

55. Schoemans, H.M., Lee, S.J., Ferrara, J.L., Wolff, D., Levine, J.E., Schultz, K.R., Shaw, B.E., Flowers, M.E., Ruutu, T., Greinix, H., et al. (2018). EBMT-NIH-CIBMTR Task Force position statement on standardized terminology & guidance for graft-versus-host disease assessment. Bone Marrow Transplant. *53*, 1401–1415. https://doi.org/10.1038/s41409-018-0204-7.

56. Wu, Z., Lamao, Q., Gu, M., Jin, X., Liu, Y., Tian, F., Yu, Y., Yuan, P., Gao, S., Fulford, T.S., et al. (2024). Unsynchronized butyrophilin molecules dictate cancer cell evasion of Vγ9Vδ2 T-cell killing. Cell. Mol. Immunol. *21*, 362–373. https://doi.org/10.1038/s41423-024-01135-z.

57. Chen, S., Zhou, Y., Chen, Y., and Gu, J. (2018). fastp: an ultra-fast all-in-one FASTQ preprocessor. Bioinformatics *34*, i884–i890. https://doi.org/10.1093/bioinformatics/bty560.

58. Dobin, A., Davis, C.A., Schlesinger, F., Drenkow, J., Zaleski, C., Jha, S., Batut, P., Chaisson, M., and Gingeras, T.R. (2013). STAR: ultrafast universal RNA-seq aligner. Bioinformatics *29*, 15–21. https://doi.org/10.1093/bioinformatics/bts635.

59. Liao, Y., Smyth, G.K., and Shi, W. (2014). featureCounts: an efficient general purpose program for assigning sequence reads to genomic features. Bioinformatics *30*, 923–930. https://doi.org/10.1093/bioinformatics/btt656.

60. Love, M.I., Huber, W., and Anders, S. (2014). Moderated estimation of fold change and dispersion for RNA-seq data with DESeq2. Genome Biol. *15*, 550. https://doi.org/10.1186/s13059-014-0550-8.

61. Yu, G., Wang, L.G., Han, Y., and He, Q.Y. (2012). clusterProfiler: an R package for comparing biological themes among gene clusters. Omics *16*, 284–287. https://doi.org/10.1089/omi.2011.0118.

62. Subramanian, A., Tamayo, P., Mootha, V.K., Mukherjee, S., Ebert, B.L., Gillette, M.A., Paulovich, A., Pomeroy, S.L., Golub, T.R., Lander, E.S., et al. (2005). Gene set enrichment analysis: a knowledge-based approach for interpreting genome-wide expression profiles. Proc. Natl. Acad. Sci. USA *102*, 15545–15550. https://doi.org/10.1073/pnas.0506580102.

63. Mootha, V.K., Lindgren, C.M., Eriksson, K.F., Subramanian, A., Sihag, S., Lehar, J., Puigserver, P., Carlsson, E., Ridderstråle, M., Laurila, E., et al.

(2003). PGC-1alpha-responsive genes involved in oxidative phosphorylation are coordinately downregulated in human diabetes. Nat. Genet. *34*, 267–273. https://doi.org/10.1038/ng1180.

64. Vabret, N., Britton, G.J., Gruber, C., Hegde, S., Kim, J., Kuksin, M., Levantovsky, R., Malle, L., Moreira, A., Park, M.D., et al. (2020). Immunology of COVID-19: Current State of the Science. Immunity *52*, 910–941. https://doi.org/10.1016/j.immuni.2020.05.002.

65. Hao, Y., Stuart, T., Kowalski, M.H., Choudhary, S., Hoffman, P., Hartman, A., Srivastava, A., Molla, G., Madad, S., Fernandez-Granda, C., et al. (2024). Dictionary learning for integrative, multimodal and scalable single-cell analysis. Nat. Biotechnol. *42*, 293–304. https://doi.org/10.1038/s41587-023-01767-y.

66. Korsunsky, I., Millard, N., Fan, J., Slowikowski, K., Zhang, F., Wei, K., Baglaenko, Y., Brenner, M., Loh, P.R., and Raychaudhuri, S. (2019). Fast, sensitive and accurate integration of single-cell data with Harmony. Nat. Methods *16*, 1289–1296. https://doi.org/10.1038/s41592-019-0619-0.

67. Zhou, Y., Zhou, B., Pache, L., Chang, M., Khodabakhshi, A.H., Tanaseichuk, O., Benner, C., and Chanda, S.K. (2019). Metascape provides a biologist-oriented resource for the analysis of systems-level datasets. Nat. Commun. *10*, 1523. https://doi.org/10.1038/s41467-019-09234-6.

68. Wu, W., Zhou, Q., Masubuchi, T., Shi, X., Li, H., Xu, X., Huang, M., Meng, L., He, X., Zhu, H., et al. (2020). Multiple Signaling Roles of CD3epsilon and Its Application in CAR-T Cell Therapy. Cell *182*, 855–871.e23. https://doi.org/10.1016/j.cell.2020.07.018.

Please cite this article in press as: Wu et al., Glycan shielding enables TCR-sufficient allogeneic CAR-T therapy, Cell (2025), https://doi.org/10.1016/j.cell.2025.07.046

STAR★METHODS

KEY RESOURCES TABLE

REAGENT or RESOURCE	SOURCE	IDENTIFIER
Antibodies		
T-Select HLA-A*02:01 CMV pp65 Tetramer-NLVPMVATV-PE	MBL	Cat# TS-0010-1C
PE anti-human CD5 Antibody (UCHT2)	Biolegend	Cat# 300608; RRID: AB_314094
Brilliant Violet 510™ anti-human CD56 (NCAM) Antibody (HCD56)	Biolegend	Cat# 318340; RRID: AB_2561944
APC anti-human HLA-A,B,C Antibody (W6/32)	Biolegend	Cat# 311410; RRID: AB_314879
PerCP/Cyanine5.5 anti-human CD3 Antibody (UCHT1)	Biolegend	Cat# 300430; RRID: AB_893299
APC anti-human HLA-E Antibody (3D12)	Biolegend	Cat# 342606; RRID: AB_2565261
APC/Cyanine7 anti-human HLA-A2 Antibody (BB7.2)	Biolegend	Cat# 343310; RRID: AB_2561568
Brilliant Violet 711™ anti-human CD45 Antibody (HI30)	Biolegend	Cat# 304050; RRID: AB_2563466
PE/Cyanine7 anti-mouse CD45 Antibody (30-F11)	Biolegend	Cat# 103114; RRID: AB_312979
FITC anti-mouse CD45.1 Antibody (A20)	Biolegend	Cat# 110706; RRID: AB_313495
PE anti-mouse CD45.2 Antibody (104)	Biolegend	Cat# 109808; RRID: AB_313445
PE anti-mouse CD3ε Antibody (145-2C11)	Biolegend	Cat# 100308; RRID: AB_312673
Brilliant Violet 785™ anti-mouse CD4 Antibody (RM4-5)	Biolegend	Cat# 100552; RRID: AB_2563053
FITC anti-mouse CD8a Antibody (53-6.7)	Biolegend	Cat# 100706; RRID: AB_312745
Biotin anti-mouse CD90.2 (Thy1.2) Antibody (30-H12)	Biolegend	Cat# 105304; RRID: AB_313175
PerCP/Cyanine5.5 anti-mouse TCR β chain Antibody (H57-597)	Biolegend	Cat# 109228; RRID: AB_1575173
PE anti-mouse H-2Kb Antibody (AF6-88.5)	Biolegend	Cat# 116508; RRID: AB_313735
PE anti-mouse H-2Db Antibody (KH95)	Biolegend	Cat# 111507; RRID: AB_313512
PE/Cyanine7 anti-mouse H-2Kd Antibody (SF1-1.1)	Biolegend	Cat# 116622; RRID: AB_2562733
Purified rat anti-mouse CD16/CD32 (2.4G2)	BD Bioscience	Cat# 553142; RRID: AB_394656
PE/Cyanine7 anti-human HLA-DR, DP, DQ Antibody (Tü39)	Biolegend	Cat# 361708; RRID: AB_2564279
PE anti-human CD58 Antibody (TS2/9)	Biolegend	Cat# 981702; RRID: AB_3083238
PE Mouse IgG1, κ Isotype Ctrl (MOPC-21)	Biolegend	Cat# 981804; RRID: AB_3076354
PE Mouse IgG2a, κ Isotype Ctrl (MOPC-173)	Biolegend	Cat# 981910; RRID: AB_2924692
APC anti-human CD107a (LAMP-1) Antibody	Biolegend	Cat# 328620; RRID: AB_1279055
PE anti-human CD95 Antibody (REA738)	Miltenyi Biotec	Cat# 130-113-004; RRID: AB_2725916
Recombinant Human NKp46/NCR1 Fc Chimera Protein	R&D Systems	Cat# 1850-NK
Recombinant Human CD2 Fc Chimera Protein	R&D Systems	Cat# 1856-CD
Recombinant Human NKG2D Fc Chimera Protein	R&D Systems	Cat# 1299-NK; RRID:AB_3083731

(*Continued on next page*)

Continued

REAGENT or RESOURCE	SOURCE	IDENTIFIER
Recombinant Human IgG1 Fc Protein	R&D Systems	Cat# 110-HG; RRID:AB_276244
PE anti-human B7-H6 Antibody	R&D Systems	Cat# FAB7144P; RRID: AB_3652285
Monoclonal Anti-FMC63 Antibody	ACROBiosystems	Cat# FM3-Y45; RRID: AB_3676237
Purified anti-Human CD3 (OKT3)	Biolegend	Cat# 317302; RRID: AB_571927
APC Annexin V	Biolegend	Cat# 640919
Anti-Signal peptide peptidase-like 3 Antibody (7F9)	Sigma-Aldrich	Cat# MABS1910
Bacterial and virus strains		
NEB Stable Competent *E. coli*	New England BioLabs	C3040H
Biological samples		
PBMCs from the patients	This study	N/A
Tissues from experimental animals	This study	N/A
Chemicals, peptides, and recombinant proteins		
Human T-Activator CD3/CD28 Dynabeads	ThemoFisher	11132D
Mouse T-Activator CD3/CD28	ThemoFisher	11453D
RPMI-1640 media	Gibco	11875093
Streptavidin Nanobeads	Biolegend	480016
Penicillin- Streptomycin	Gibco	15070063
X-VIVO™ 15 media	Lonza	02-053Q
sodium propionate	Sigma-Aldrich	P1880
Human CMV pp65 (495-503) peptide	Sangon	T510162-0001
X-tremeGENE™ HP DNA Transfection Reagent	Roche	06366236001
Protease K	NEB	P8107S
Recombinant Human Interleukin-2 for Injection	Sihuan Shengwu	N/A
CFSE Cell Division Tracker Kit	Biolegend	423801
CellTrace™ Violet (CTV) Cell Proliferation Kit	ThermoFisher	C34571
7-AAD Viability Staining Solution	Biolegend	Cat#420404
DAPI (4',6-Diamidino-2-Phenylindole, Dilactate)	Biolegend	Cat# 422801
Recombinant Human FASL (TNFSF6)	Biolegend	Cat# 589402
Precision Count Beads™	Biolegend	424902
Concanavalin A (Con A)	Vector Laboratories	FL-1001-25
Lycopersicon Esculentum Lectin (LEL)	Vector Laboratories	FL-1171-1
Sambucus Nigra Lectin (SNA)	Vector Laboratories	L-1300-5
PNGase F	NEB	P0704
O-Glycoprotease (IMPa)	NEB	P0761S
Trypsin/Lys-C Mix, Mass Spec Grade	Promega	V5071
Critical commercial assays		
Mouse CD 3 T Cell Isolation Kit	Biolegend	480024
Human T Cell Isolation Kit	Stemcell	17951
Human NK Cell Isolation Kit	Stemcell	17955
Human Th1/Th2/Th17 CBA Kit	BD Biosciences	560484
DNeasy Blood & Tissue Kits	QIAGEN	69504
Quick-RNA™ MicroPrep	Zymo	R1050

(*Continued on next page*)

Please cite this article in press as: Wu et al., Glycan shielding enables TCR-sufficient allogeneic CAR-T therapy, Cell (2025), https://doi.org/10.1016/j.cell.2025.07.046

Continued

REAGENT or RESOURCE	SOURCE	IDENTIFIER
Deposited data		
Raw LC-MS files	https://www.proteomexchange.org/	PXD052748
Raw RNA-seq files	https://ngdc.cncb.ac.cn/	PRJCA040498
Experimental models: Cell lines		
Jurkat T cells	Dr. H. Wang (ShanghaiTech University)	N/A
Nalm6 cells	Procell	CL-0701
HEK293T	Procell	CL-0005
HLA-A*02:01 CMV pp65-specific T cells	This study	N/A
Anti-CD19 CAR T cells	This study	N/A
Experimental models: Organisms/strains		
NOD/ShiLtJGpt-Prkdc^{em26Cd52} Il2rge^{m26Cd22}/Gpt	GemPharmatech (Nanjing, China)	Strain #: T001475
B6	Charles River Laboratories (Beijing, China)	Strain #: 219
BALB/c	Charles River Laboratories (Beijing, China)	Strain #: 211
Oligonucleotides		
sgRNA targeting SPPL3 (5'-3': AGACAGATGCTCCAATTGGA)	GenScript	N/A
sgRNA targeting AAVS1 (5'-3': GTCACCAATCCTGTCCCTAG)	GenScript	N/A
sgRNA targeting B2M (5'-3': GAGTAGCGCGAGCACAGCTA)	GenScript	N/A
Nontargeting control sgRNA (5'-3': GCGAGGTATTCGGCTCCGCG)	GenScript	N/A
sgRNA targeting Sppl3 (5'-3': ATCGGGGACATTGTGATGCC)	GenScript	N/A
sgRNA targeting Trac (5'-3': UAUGGAUUCCAAGAGCAAUG)	GenScript	N/A
Recombinant DNA		
pR8.74	Addgene	22036
VSVg	Addgene	158233
Software and algorithms		
Living Image software	PerkinElmer	https://www.perkinelmer.com.cn/
Flowjo software	Tree Star	https://www.flowjo.com/
Graphpad	Prism	https://www.graphpad.com/
Maxquant (version 1.6.15.0)	https://www.maxquant.org/	https://pubmed.ncbi.nlm.nih.gov/19029910/
Byonic (version 5.3.5)	Protein Metrics Inc.	https://www.proteinmetrics.com/products/byonic
Xcalibur (version 4.3)	Thermo Fisher Scientific	https://www.thermofisher.com/order/catalog/product/OPTON-30965
Biorender	Biorender	https://www.biorender.com/
Other		
BTX Electroporation Cuvettes Plus, 4 mm	BTX	45-0142
Immunostainer	DAKO	Leica Bond-III

Please cite this article in press as: Wu et al., Glycan shielding enables TCR-sufficient allogeneic CAR-T therapy, Cell (2025), https://doi.org/10.1016/j.cell.2025.07.046

EXPERIMENTAL MODEL AND STUDY PARTICIPANT DETAILS

Clinical trials design

This study was a phase 1, open-label, single-arm clinical trial designed to evaluate the safety and efficacy of anti-CD19 allogeneic SPPL3^{KO}/TCR^{KO} CAR-T cells in treating aggressive relapsed/refractory B-cell non-Hodgkin lymphoma (B-NHL). The protocol was finalized and received ethical approval in July 2023. The trial was officially registered (NCT06014073) in August 2023. Enrollment began in September 2023, starting with the first patient (including one compassionate use case), and concluded with the final patient enrollment in March 2024. The inclusion criteria were as follows: (1) age between 18 and 70 years; (2) diagnosis of CD19+ relapsed/refractory B-NHL, including diffuse large B-cell lymphoma not otherwise specified, primary mediastinal large B-cell lymphoma, transformed follicular lymphoma, high-grade B-cell lymphoma with MYC and BCL2 and/or BCL6 rearrangements, follicular lymphoma, mantle cell lymphoma, and marginal zone lymphoma; (3) life expectancy of more than 3 months; (4) Eastern Cooperative Oncology Group (ECOG) score of 2 or lower and satisfactory major organ functions; and (5) negative pregnancy test for women of reproductive potential and agreement to use birth control during the study. The exclusion criteria included: (1) pregnancy or breastfeeding; (2) autologous stem cell transplant with therapeutic intent within 3 months of planned SPPL3^{KO}/TCR^{KO} anti-CD19 CAR-T cell infusion; (3) history of allogeneic stem cell transplantation; (4) prior CD19 targeted therapy; (5) active autoimmune disease requiring immunosuppressive agents; (6) active infection; (7) history of other malignancies; and (8) ineligibility or inability to comply with the study requirements. In the dose escalation stage, enrolled subjects in each cohort will be randomly assigned to receive SPPL3^{KO}/TCR^{KO} anti-CD19 CAR-T cell infusion from different donors. Dosing will proceed in a stepwise fashion, starting at dose level 1 (1×10^6/kg) using a traditional 3 + 3 dose escalation model. The therapy includes 3 days of lymphodepletion chemotherapy using combined fludarabine (30-50 mg/m^2 from days -5 to -3) and cyclophosphamide (500-1000 mg/m^2 from days -5 to -3). CAR-T cell infusion is performed 2 days after the end of lymphodepletion chemotherapy and is followed by standard monitoring. Baseline characteristics of patients are shown in Table S1. During the screening phase, several patients were excluded based on predefined criteria: Patient 01 due to a history of autologous CAR-T cell therapy, Patient 08 because of pulmonary insufficiency that could compromise safety assessments, and Patient 13 for active pulmonary fungal and COVID-19 infections. Patient 16 was excluded for active hepatitis B virus infection, Patient 18 due to central nervous system lymphoma, and Patient 19 for lacking measurable lesions. Patient 10 remained under screening at the data cutoff. These exclusions were necessary to maintain study integrity and participant safety. Patient 12 withdrew consent, Patients 07, 14, and 15 died from disease progression during screening. Three batches of cell products were successfully manufactured, with C23002 (male donor) showing 99.78% TCR negativity, 99.06% SPPL3 editing, 42.02% CAR positivity, and a CD4:CD8 ratio of 1.41; C23003 (male donor) demonstrating 99.76% TCR negativity, 98.84% SPPL3 editing, 52.65% CAR positivity, and a CD4:CD8 ratio of 0.88; and C23004 (female donor) exhibiting 99.93% TCR negativity, 99.23% SPPL3 editing, 50.49% CAR positivity, and a CD4:CD8 ratio of 0.84. All batches met the required quality specifications for therapeutic use.

The primary endpoints of the study were dose-limiting toxicities (DLTs) within 28 days and determining the recommended phase II dose (RP2D). DLT is defined as any adverse event (AE) related to the SPPL3^{KO}/TCR^{KO}/anti-CD19 CAR-T that occurs within 28 days after infusion and meets any one of the follow criteria: (1) $\geq$ Grade 3 aGVHD that does not resolve to Grade 1 or 2 within 7 days, with the exception of isolated skin involvement aGVHD; (2) $\geq$ Grade 4 cytokine release syndrome (CRS) or grade 3 CRS that does not resolve to grade 2 or lower within 2 weeks; (3) Grade 3 immune effector cell-associated neurotoxicity syndrome (ICANS) lasting for $\geq$ 7 days or Grade 4 ICANS; (4) Any other AEs associated with CAR-T and lasting $\geq$ 14 days of grade 3 and above except hematological toxicity. The RP2D was based on a combination of a similar safety profile across dose levels ($\leq$ maximum tolerated dose), CAR$^+$ T cell expansion kinetics, and antitumor activity. The maximum tolerated dose is defined as the highest dose level at which the incidence of DLT is $\leq$ 30%. The secondary endpoints included objective response rate (ORR), complete response (CR) rate, pharmacokinetics, and pharmacodynamics, progression-free survival (PFS) and overall survival (OS). The ORR was defined as the proportion of patients who achieved either a CR or partial response (PR). The CR rate was defined as the proportion of patients achieving a CR. PFS was defined as the time from SPPL3^{KO}/TCR^{KO}/anti-CD19 CAR-T infusion to the first assessment of progressive disease (PD) or death from any cause. OS was defined as the period from SPPL3^{KO}/TCR^{KO}/anti-CD19 CAR-T infusion to until the date of death from any cause or the date of the last survival follow-up visit. Grading of CRS and ICANS will be performed according to the American Society for Transplantation and Cellular Therapy (ASTCT) Consensus. Acute GvHD will be assessed using the Mount Sinai Acute GvHD International Consortium (MAGIC) criteria, while all other adverse events will be evaluated according to the CTCAE v5.0 criteria. The efficacy assessment assessed by investigators according to the Lugano 2014 criteria.

The study protocol for the Phase I clinical trial of TCR-sufficient SPPL3^{KO}/anti-CD19 CAR-T cells was finalized and approved by the ethics committee of the Chinese PLA General Hospital in February 2024, with formal trial registration completed in March 2024. The full protocol is publicly available in the ClinicalTrials.gov registry. Three patients who received TCR-sufficient CAR-T cells under compassionate-use provisions. All participants provided written informed consent prior to enrollment, in accordance with the principles of the Declaration of Helsinki. Two batches of TCR-sufficient CAR-T cells were successfully manufactured: C23003 (male donor) achieved 96.88% SPPL3 editing efficiency with 44.76% CAR expression and a CD4:CD8 ratio of 0.65, while C23007 (male donor) showed 98.87% SPPL3 editing with 71.62% CAR expression and a CD4:CD8 ratio of 0.8.

The patients of two studies consisted of 7 females and 6 males, all of East Asian ancestry (Han Chinese).

Please cite this article in press as: Wu et al., Glycan shielding enables TCR-sufficient allogeneic CAR-T therapy, Cell (2025), https://doi.org/10.1016/j.cell.2025.07.046

Extended clinical details for SPPL3^{KO}/TCR^{KO} CAR-T cell therapy

The infusion of allogeneic residual CD3$^+$ T cells harboring grafts was limited to a maximum of 2×10^5 per kilogram for each recipient. Prior to CAR-T cell infusion, patients underwent a lymphodepletion regimen comprising fludarabine (30-50 mg/m^2 per day) and cyclophosphamide (500-1000 mg/m^2 per day) administered on days -5, -4, and -3 (Figure S3A). To ensure consistency, enrolled subjects within each cohort were randomly assigned to receive *SPPL3*^{KO}/TCR^{KO}/anti-CD19 CAR-T cells from healthy donors (Figure 5A). For managing CRS and ICANS (Figure S3C), 66.7% of patients received tocilizumab (median cumulative dose: 400 mg; range: 320–800 mg), 22.2% received glucocorticoids, 88.9% received infliximab, 22.2% were treated with vasopressors, and 55.6% underwent therapeutic plasma exchange.

Extended clinical details for SPPL3^{KO} CAR-T cell therapy

The Patient C01 had a history of classical Hodgkin lymphoma, but only non-Hodgkin lymphoma was detected in the baseline biopsy. Elevated serum creatinine levels (160 μmol/L) excluded her from standard trial inclusion criteria. Additionally, her low white blood cell counts during screening made her ineligible for autologous CAR-T cell collection. After informed consent, she was treated under compassionate use. Her kidney lesions showed a tumor burden SPD of 59.4 cm^2. The patient underwent a lymphodepletion regimen of fludarabine (30 mg/m^2/day, days -5 to -3) and cyclophosphamide (500 mg/m^2/day, days -5 to -3), followed by a single infusion of SPPL3^{KO} anti-CD19 CAR-T cells at 6×10^6/kg. Management included infliximab (300 mg on days 1 and day 4), tocilizumab (400 mg on day 2), methylprednisolone (80 mg), inflammatory factor adsorption, tacrolimus (0.5 mg on day 5), and ruxolitinib (10 mg on day 5), followed by therapeutic plasma exchange on day 6. Tacrolimus and ruxolitinib were used to suppress HvG reactions.

Patient C02, a 27-year-old woman diagnosed with primary mediastinal large B-cell lymphoma in March 2020, experienced disease progression despite five prior lines of systemic therapy. Her disease involved the left lung, mediastinum, and peripheral lymph nodes, with a baseline tumor burden SPD of 94.3 cm^2. Due to tumor compression causing left lung atelectasis and type I respiratory failure, excluded her from standard trial inclusion criteria. After informed consent, she was treated under compassionate use. Following cytoreductive therapy with polatuzumab vedotin on day –10, she received a lymphodepletion regimen of fludarabine (40 mg/m^2/day) and cyclophosphamide (600 mg/m^2/day) from day –5 to –3. A single infusion of *SPPL3*^{KO} CAR-T cells (6×10^6/kg) was administered. Management of CRS included infliximab (300 mg, day 1), tocilizumab (400 mg, day 2), plasma exchange (days 3 and 5), and ruxolitinib to suppress HvG reactions (5 mg BID on day 5, then once daily on day 6). The patient experienced a grade 3 pulmonary fungal infection, which improved after intravenous voriconazole treatment. Apart from hematologic toxicity, all other adverse events resolved.

Patient C03, a 34-year-old male with high-risk mixed lineage leukemia (MLL)–rearranged B-ALL, was diagnosed in August 2023 with an initial marrow blast count of 76.82%. He achieved complete remission with incomplete blood count recovery (CRi) after first-line chemotherapy but remained minimal residual disease (MRD) positive. On April, 2024, he received autologous anti-CD19 CAR-T cells following fludarabine (30 mg/m^2/day) and cyclophosphamide lymphodepletion (300 mg/m^2/day) for 3 days, achieving MRD-negative CRi at one month. However, relapse occurred at eight months post-treatment with 87.97% CD19$^+$ blasts and undetectable CAR VCN. During the screening period, the patient presented with uncontrolled fungal pneumonia and bacterial lower limb infection, which did not meet the inclusion criteria. After informed consent, he was treated under compassionate use. Before allogeneic CAR-T therapy, the patient received cytoreductive chemotherapy (vincristine, daunorubicin, cyclophosphamide, L-asparaginase, and methotrexate), reducing MRD to 4.03% by day –14. Lymphodepletion (fludarabine 30 mg/m^2/day and cyclophosphamide 500 mg/m^2/day, days –5 to –3) brought MRD down to 0.69% by day –1. He then received 6×10^6/kg *SPPL3*^{KO} CAR-T cells.

Animals

NOD/ShiLtJGpt-Prkdc^{em26Cd52}Il2rge^{m26Cd22}/Gpt mice (NCG) were purchased from GemPharmatech (Nanjing, China). B6 and BALB/c mice were ordered from Charles River Laboratories (Beijing, China). All mice used in the study were housed and bred under specific pathogen-free conditions and handled in accordance with the guidelines of the Peking University Institute of Systems Biomedicine. Six- to eight-week-old mice were randomly assigned to experimental groups. Both male and female mice were used. For NK cell killing experiments, 100,000 IU IL2 and 20 million NK cells were injected into the animals. The following day, 4 million barcoded T cells were injected, and the ratios of *SPPL3*^{KO} cells and *AAVS1*^{KO} cells were determined 24 hours later. To establish a xenograft tumor model, mice were injected with Nalm6 cells (1×10^6). The mice were then randomly divided into experimental and control groups. CAR-T cells were injected into the mice via tail vein injection. The survival of the mice was monitored, and the tumor was tracked using bioluminescence imaging. The photons emitted from luciferase-expressing cells were quantified using Living Image software (PerkinElmer). A total body region of interest was drawn around each mouse, and radiance was recorded in units of photons/s/cm^2/sr. Mouse CD3 T cells were isolated from the spleens of B6 mice following the manufacturer's instructions (BioLegend). The T cells were then activated by the anti-CD3/CD28 beads for 48 hours (Thermo Fisher Scientific). Cas9 mRNA and single-guide RNA were electroporated using MaxCyte system. The cells were rested at 37°C for one day, harvested, and expanded in RPMI-1640 media (Gibco) with 100IU hIL-2 (IL-2; Sihuan ShengWu) for another week. For transfer experiments, the mice were irradiated using an X-ray generator SR200 (SCIRAY, Changzhou, China). GvHD symptoms were assessed by a published scoring system.[53]

Please cite this article in press as: Wu et al., Glycan shielding enables TCR-sufficient allogeneic CAR-T therapy, Cell (2025), https://doi.org/10.1016/j.cell.2025.07.046

Cell lines

Jurkat T cells were obtained from Dr. H. Wang (ShanghaiTech University) and maintained in RPMI 1640 medium. Nalm6 cells were used as the target cells for anti-CD19 CAR-T cells. All media were supplemented with 10% fetal bovine serum (FBS), penicillin, and streptomycin (Gibco).

Primary cells

Peripheral blood mononuclear cells (PBMCs) were collected from de-identified healthy donor apheresis products, isolated by Ficoll purification, and stored in liquid nitrogen prior to experimentation. Primary T cells and NK cells were purified using a negative selection kit (STEMCELL Technologies) and expanded in X-VIVO™ 15 media (Lonza) with 100 IU/ml interleukin-2. When applicable, primary T cells were subjected to an overnight treatment with 10 mM sodium propionate (Sigma-Aldrich) and subsequently utilized as the targets for NK cells. HLA-A*02:01 CMV pp65-specific T cells were expanded using a synthesized peptide (NLVPMVATV, Sangon) at a concentration of 2 μg/ml. The cells were then stained for positivity using an HLA-A2/NLV recognizing tetramer.

METHOD DETAILS

Assessment of response

Treatment response was assessed according to the revised criteria of the Lugano 2024 classification. PET-CT scans and bone marrow biopsy were the main methods used to evaluate lymphoma lesions. The response assessment criteria were as follows: (1) CR (complete remission): absence of clinical symptoms, PET-CT, and bone marrow evidence associated with lymphoma; (2) PR (partial remission): lymphoma volume decrease of at least 50% without new lymphoma lesions or sustained bone marrow involvement; (3) PD (progressive disease): lymphoma volume increase of at least 50% or onset of new lymphoma lesions; (4) SD (stable disease): a condition that does not meet the criteria for CR, PR, or PD. The evaluation data for Cohort 2 is updated and valid up to March 31, 2025. For B-ALL patient, CR was defined as less than 5% bone marrow blasts, the absence of circulating blasts, and no extramedullary sites of disease (as assessed by means of computed tomography or positron-emission tomography), regardless of cell count recovery. A negative status for minimal residual disease was defined as less than 0.01% bone marrow blasts, as assessed by means of multiparameter flow cytometry.

Assessment and grading of CRS

Serum cytokines, including IL-1, IL-2, IL-6, IL-8, IL-10, ferritin, TNF-α, and IFN-γ, were assessed using the Human Th1/Th2/Th17 CBA kit (BD Biosciences) within 1 month of infusion. CRS was assessed and graded according to the standards released by the American Society for Transplantation and Cellular Therapy (ASTCT) in 2019.[54] Among the nine patients, six patients were treated with tocilizumab, eight patients were treated with infliximab, and only two patients were treated with glucocorticoids.

Assessment and grading of ICANS

ICANS was assessed and graded according to the standards released by the ASTCT in 2019.[54] Once CRS symptoms such as pyrexia, hypotension and capillary leak or other types of AEs were observed, the patient would be closely monitored for signs of neurological toxicity, such as seizure, tremor, encephalopathy or dysphasia.

Assessment and grading of GvHD

GvHD was assessed and graded according to the criteria defined by the Mount Sinai Acute GvHD International Consortium.[55] The acute GvHD classification criteria were based on the clinical manifestations of target organ involvement, including the skin, gut, and liver.

Assessment and grading of adverse events (AEs)

Patients were admitted as inpatients and closely monitored after receiving lymphodepletion chemotherapy and CAR-T cell infusion. Physical and clinical laboratory examinations were documented during hospitalization to evaluate the toxicity of the treatment. AEs were graded using NCI-CTCAE version 5.0. All AEs are summarized in Table S2. Any AEs that occurred after CAR-T cell infusion during hospitalization were recorded. Severe AEs, except for a decrease in lymphocyte counts caused by lymphodepletion chemotherapy, were required to be reported to the Medical Ethics Committee of The First Medical Center, Chinese PLA General Hospital within 24 hours of occurrence. One month after infusion, patients underwent follow-up and were monitored for disease progression and toxicity once a month thereafter.

Bidirectional Allogeneic T-Cell Reaction Syndrome (BATCRS)

Unlike classical unidirectional immune responses such as GvHD or HvG rejection, BATCRS is characterized by localized inflammation without causing pathological tissue damage. Clinically, BATCRS typically manifests with transient head and neck edema, rash, or diarrhea—often preceding the onset of fever seen in conventional CRS. Notably, BATCRS responds poorly to standard CRS treatments such as tocilizumab (IL-6 blockade) or infliximab (TNF-α inhibition), reflecting its distinct underlying mechanistic. Whereas classical CRS is driven by monocyte-macrophage activation and IL-6 production, BATCRS arises from reciprocal T-cell interactions

Please cite this article in press as: Wu et al., Glycan shielding enables TCR-sufficient allogeneic CAR-T therapy, Cell (2025), https://doi.org/10.1016/j.cell.2025.07.046

and is predominantly mediated by IL-2. Recognizing this mechanistic distinction is critical to avoid ineffective IL-6-targeted therapies and delays in appropriate management. In patients receiving allogeneic *SPPL3*^{KO} CAR-T therapy, BATCRS often occurs concurrently with CRS, underscoring the need for early identification based on its unique clinical features. Importantly, BATCRS is typically self-limiting and resolves with supportive care alone, highlighting its classification as a distinct clinical syndrome and underscoring its relevance in optimizing therapeutic strategies for allogeneic cell therapies.

Cytotoxicity assessment

To evaluate the cytotoxic activity of CAR-T cells, Nalm6 cells transduced with luciferase were co-cultured with effector cells at varying ratios. Cytolysis was quantified by introducing 150 μg/ml d-luciferin (PerkinElmer). Luciferase bioluminescence was subsequently measured using a luminometer.

Generation of engineered T-cells

Knockout T cells were generated using CRISPR-Cas9 technology. Anti-CD3/CD28 beads (ThermoFisher) activated T cells were electroporated with sgRNA and Cas9 mRNA (synthesized by TriLink) in a 4 mm BTX electroporation cuvette. T cells post-electroporation were transferred into a T150 cell culture flask, supplemented with X-VIVO™ 15 media (Lonza) to adjust cell density to 1×10^6 cells/mL. Passages of cells were conducted every two days. The KO efficiency was evaluated by a sequencing-based assay. When applicable, anti-CD3/CD28-stimulated T cells were retrovirally transduced with anti-CD19 CAR. The expression of CAR-T cells was determined 6-9 days post-transduction, and experiments were performed 6-14 days post-transduction.

Lentiviral production and infection

Lentivirus was produced by transfecting HEK293T cells with a lentiviral transfer vector, the packaging plasmid pR8.74 (#22036; Addgene), and VSVg (#158233; Addgene) using X-tremeGENE HP DNA transfection reagent (Roche). The viral supernatant was collected 72 hours after transfection, purified by passing it through a 0.45-μm filter, and added to target cells along with 8 μg/ml polybrene.

Indel analysis

The breast tissue was digested using a 1% SDS lysis buffer with protease K to obtain genomic DNA. The genomic DNA was then isolated through isopropanol precipitation. Fragments containing indel sites were amplified by PCR using specific primers. The PCR products were sent for library preparation and next-generation sequencing by Beijing Tsingke Biotech. The indel percentage was calculated through bioinformatic analysis.

Genome-wide CRISPR screen, functional enrichment analysis

The screening experiments using the CRISPR sgRNA^{iBAR} library were conducted as previously described.[56] T cells were infected with a pooled lentiviral genome-wide sgRNA library at a multiplicity of infection of three. After Cas9-mRNA electroporation, the cells were prepared for screening at day 7. For each screening experiment, the harvested cells were divided into a control group and an experimental group, which were maintained at a minimum coverage of 1000X. The control group cells were passaged every two days. In the NK killing screen experiment, NK cells were introduced to the co-culture at an effector-to-target (E:T) ratio of 1:8 for two consecutive rounds of killing, with each round lasting for 72 hours. The cells resistant to NK killing were expanded for an additional three days between the two rounds of NK-cell treatment. In the HLA-ABC screen, T cells with low abundance of HLA-ABC were sorted for sequencing. In the FasL screen, T cells were treated with FasL at a concentration of 10 ng/ml for 3 rounds, with each round lasting for 24 hours. The cells resistant to FasL killing were expanded for an additional 3 days between the multiple rounds of FasL treatment. Genomic DNA was extracted, and next-generation sequencing (NGS) was performed by GENEWIZ. Paired-end sequencing reads were used to extract both sgRNA and iBar (sgRNA^{iBar}) sequences. The MAGeCK^{iBAR} analysis pipeline was applied to calculate the positive screening scores of all targeted genes. Gene annotations were retrieved from the UCSC hg38 genome, which includes 19,210 genes. For each gene, three different sgRNAs with four barcodes were designed using the DeepRank algorithm. A thousand non-targeting sgRNAs, each with four barcodes, were used as negative controls.

Flow cytometry based competitive killing assay

T cells were labeled with either CTV or CFSE at a 1:1000 dilution in PBS for 5 minutes at room temperature. The dyes were quenched with media containing 10% FBS. Barcoded T cells were mixed at a 1:1 ratio and subjected to treatment with FasL, NK cells, or T cells. The ratios of cells of interest were measured by flow cytometry and compared with the results of the untreated group.

RNA-seq analysis

RNA was isolated from CAR-T cells using Quick-RNA™ MicroPrep (Zymo) according to manufacturer protocol, followed by cDNA synthesis, amplification and library preparation (Vazyme). Paired-end Illumina next-generation sequencing was performed for RNA-seq. Quality control of the sequencing data was conducted using FastQC (v0.11.9, http://www.bioinformatics.babraham.ac.uk/projects/fastqc/). Adapters were removed using fastp (v0.12.4) with default parameters.[57] The reads were then aligned to the GRCh38.p14 reference genome using the STAR aligner (v2.5.2b).[58] Gene expression levels were quantified with featureCounts

(v2.0.1).[59] For principal component analysis (PCA), the varianceStabilizingTransformation (VST) method from DESeq2 (v1.26.0) was employed, selecting the top 2,500 genes with the highest dispersion.[60] Gene Set Enrichment Analysis (GSEA) was performed using the clusterProfiler package (v3.14.3) in R (v3.6.3),[61] with gene sets sourced from the Molecular Signatures Database (MSigDB) (v2023.2, PMID 16199517, 12808457).[62,63] The following pathways were utilized for the transcription features: Exhaustion: EXHAUSTION_HUMAN_ESG_ATAC_UP,[64] proliferation: GOBP_POSITIVE_REGULATION_OF_T_CELL_PROLIFERATION, activation: GOBP_REGULATION_OF_T_CELL_ACTIVATION, apoptotic process: GOBP_T_CELL_APOPTOTIC_PROCESS, differentiation: GOBP_T_CELL_DIFFERENTIATION.

We employed custom R scripts along with Seurat version 5.0.3 for processing scRNA-Seq data.[65] Initially, we filtered out cells with fewer than 500 detected genes and with mitochondrial gene UMI counts exceeding 10% of total UMIs. The remaining high-quality gene-by-cell count matrices were merged to create a comprehensive matrix, which was then converted into a Seurat object for further analysis. Data normalization was performed using the *NormalizeData* function in Seurat. We identified the top 2,000 variably expressed genes (VEGs) utilizing the *FindVariableFeatures* function with default settings, excluding any VEGs expressed in less than 1% of cells from further analysis. For data integration, we applied the *RunHarmony* function by sample identifier, facilitating the integration of normalized expression matrices.[66] We then identified differentially expressed genes (DEGs) within the CAR +TCR- population across various time points, using an adjusted p-value threshold of <0.05 and a log2 fold change (FC) greater than 0.5. Gene ontology enrichment was analyzed using Metascape.[67] Finally, gene signature scores were calculated using the AddModuleScore function in the Seurat package.

Immunohistochemistry

Immunohistochemistry (IHC) analysis was performed on formalin-fixed, paraffin-embedded tissue sections. Briefly, the sections were deparaffinized in xylene and rehydrated in a graded alcohol series. Endogenous peroxidase was blocked with 3% hydrogen peroxide. Antigen retrieval was performed using EDTA buffer (pH 9.0). After rinsing the sections in PBS, antibodies against human CD20 and CD19 were used for IHC staining. Staining was conducted on an automated immunostainer.

Cellular membrane fraction and Western Blot

The following procedure was performed to isolate crude cellular membrane fraction: 5 million T cells were washed in 1 mL of PBS. The cell pellets were then resuspended in 1 mL of hypotonic buffer (10 mM Tris, 2 mM EDTA, pH 7.6) and chilled on ice for 10 minutes. Afterward, the samples were sheared through a 26G needle 10 times and centrifuged at 720 xg (3,000 rpm) for 5 minutes at 4°C. The supernatant recovered in the previous step was centrifuged at 8,000 rpm (10,000 xg) for 5 minutes. The resulting supernatant was subjected to ultracentrifugation at 40,000 rpm (100,000 xg) for 30 minutes at 4°C, forming a visible pellet at the bottom. The obtained pellet was then lysed in 40 μL of RIPA buffer containing protease inhibitors (50 mM Tris (pH 7.4), 150 mM NaCl, 1% Triton X-100, 1% sodium deoxycholate, 0.1% SDS) on ice for 10 minutes. Finally, the sample, along with the loading buffer, was heated at 37°C for 30 minutes. A total of 20 μL of the samples were loaded onto the gel for separation. The SPPL3 detection was performed using Clone 7F9 at a concentration of 1 μg/mL.

LC-MS/MS analysis for the differentially expressed proteins

SPPL3^{KO} T cells and control T cells were prepared from two human donors. The samples were ground into cell powder using liquid nitrogen and transferred to a 5-mL centrifuge tube. Four volumes of lysis buffer (1% SDS, 1% protease inhibitor cocktail) were added to the cell powder, followed by sonication on ice for 3 minutes using a high-intensity ultrasonic processor (Scientz). The debris was removed by centrifugation at 12,000 g at 4°C for 10 minutes, and the supernatant was collected to determine the protein concentration using a BCA kit according to the manufacturer's instructions.

The protein sample was precipitated with pre-cooled acetone, washed 2-3 times, and then redissolved in 200 mM TEAB. Trypsin was added at a 1:50 trypsin-to-protein mass ratio for overnight digestion. The resulting peptides were reduced with 5 mM dithiothreitol for 30 minutes at 56°C and alkylated with 11 mM iodoacetamide for 15 minutes at room temperature in darkness. The peptides were then desalted using a Strata X SPE column. The tryptic peptides were dissolved in solvent A and directly loaded onto a home-made reversed-phase analytical column (25-cm length, 100 μm i.d.). The mobile phase consisted of solvent A (0.1% formic acid, 2% acetonitrile in water) and solvent B (0.1% formic acid in acetonitrile). Peptides were separated using the following gradient: 0-70 min, 6%-24% B; 70-84 min, 24%-32% B; 84-87 min, 32%-80% B; 87-90 min, 80% B, all at a constant flow rate of 450 nl/min on a NanoElute UHPLC system (Bruker Daltonics). The peptides were then subjected to capillary source and analyzed using a timsTOF Pro 2 mass spectrometer. The electrospray voltage applied was 1.7 kV, and the TOF detector analyzed precursors and fragments with a MS/MS scan range from 100-1700. The timsTOF Pro was operated in parallel accumulation serial fragmentation (PASEF) mode, with precursors with charge states 0-5 selected for fragmentation and 10 PASEF-MS/MS scans acquired per cycle. The dynamic exclusion was set to 30 seconds. The resulting MS/MS data were processed using MaxQuant search engine (v.1.6.15.0). Tandem mass spectra were searched against the Homo_sapiens_9606_SP_20230103.fasta database (20389 entries) concatenated with reverse decoy and contaminants. Trypsin/P was specified as the cleavage enzyme, allowing up to 2 missing cleavages. The minimum peptide length was set to 7, and the maximum number of modifications per peptide was set to 5. The mass tolerance for precursor ions was set to 20 ppm in the first search and 20 ppm in the main search, while the mass tolerance for fragment ions was set to 20

Please cite this article in press as: Wu et al., Glycan shielding enables TCR-sufficient allogeneic CAR-T therapy, Cell (2025), https://doi.org/10.1016/j.cell.2025.07.046

ppm. Carbamidomethyl on Cys was specified as a fixed modification, and acetylation on protein N-terminal and oxidation on Met were specified as variable modifications. The false discovery rate (FDR) of protein, peptide, and PSM was adjusted to <1%.

Immunoprecipitation

To analyze glycans of anti-CD19-CAR and TCR complex, 30 million *SPPL3*^{KO} T cells or control T cells were subjected to two washes with cold PBS. Subsequently, the cell pellets were resuspended in 1x lysis/IP buffer containing 0.5% digitonin, 25 mM Tris-HCL (pH7.4), 75 mM NaCl, 5 mM EDTA, 2 mM Na3VO4, 20 mM NaF and complete protease inhibitor as previously described.[68] The cell lysis process was carried out with rotation at 4°C for 30 minutes. Following lysis, OKT3 (5 μg per mL lysate) or FM3-Y45 (1.25 μg per mL lysate) monoclonal antibody was introduced, and the cell lysates were rotated for 12 hours at 4°C. Subsequently, 10 μL of Protein A/G-Sepharose beads were added to each sample, and the cell lysates were rotated at 4°C for 3 hours. After incubation, antibody-beads complex was washed three times with 200 μL of 1 x PBS and 200 μL of 0.1 x PBS. Post-washing, the captured glycoproteins were eluted using an elution buffer (0.1 M glycine-HCl, pH 2.5) at 37°C for 15 minutes, with the elution process repeated three times.

Proteolytic glycopeptides preparation

The proteins from cell lysate immunoprecipitation samples were precipitated using trichloroacetic acid (TCA) at 4°C for 6 hous and then washed twice with acetone. The collected proteins were denatured in 8 M urea and 100 mM Tris-HCl (pH 8.5) buffer, then reduced with 20 mM Tris (2-carboxyethyl) phosphine (TCEP) for 20 minutes and alkylated with 40 mM Iodoacetamide (IAA) for 30 minutes in the dark. The samples were diluted three-fold using Tris-HCl (pH 8.5) buffer and aliquoted into two tubes for N- and O-glycosylation analysis. The O-glycoprotease (IMPa, P0761S) was added and incubated at 37°C for 6 hours. Trypsin-LysC mix (Promega, mass-spectrometry grade) were sequentially added (enzyme: protein, 1:25 w/w), and incubated at 37°C for 16 hours. The peptides were cleaned up using C_{18} column cartridges (SOLAμ™, ThermoFisher) and dried using a speedvac (Labconco). For O-glycopeptides analysis, the purified peptides were additionally treated with PNGase F (P0704, NEB) in O^{18} water at 37°C for 6 hours to remove N-glycans. Followed by this, the glycopeptides were cleaned up and vacuum-centrifuged to dryness for LC-MS/MS analysis.

LC-MS/MS analysis for glycans

The glycoproteins were analyzed using the Vanquish™ Neo UHPLC system (Thermo) combined with Orbitrap Eclipse™ Tribrid MS platform (Thermo) in data-dependent acquisition (DDA) mode for site-specific glycan characterization. Mobile phase of solvent A was 0.1% formic acid in water, and solvent B was 0.1% formic acid in 80% acetonitrile (ACN). The trap column (75 μm × 2 cm, 3 μm, 100Å, Thermo) and C_{18} analytical column (7.5 μm × 25 cm, 1.9 μm, home-made) were utilized for LC separation at a flow rate of 400 nL/min. The elution gradient was optimized as follows: 2-28% B for 135, 28-45% B for 15 minutes, 45-100% B for 15 minutes, and 100% B for 15 minutes. The HCDpdEThcD mode was applied for the data acquisition. Full scan mass spectra were acquired in the range of m/z 350 to 2,000 with a resolution of 60,000 full widths at half maximum (FWHM). The normalized automatic gain control (AGC) target of precursors was set as 100%, and maximum injection time (MIT) was auto. The MS2 spectra were acquired with a mass range from m/z 100 to 1,800 at a resolution of 30,000 FWHM and normalized AGC target of 200%. The isolation window was set as m/z 1.6, and the stepped-normalized HCD collision energy (sNCE) was 15%, 30% and 45%. Product dependent EThcD was triggered if at least one of the specific ions (126.0551, 138.0545, 144.0655, 147.0657, 163.0606, 168.0655, 186.0761, 204.0867, 243.026, 292.1032, 366.1396, and 407.1665) was hit in the HCD spectra.

Database search and glycans analysis

Raw LC-MS/MS files were analyzed using Byonic (version 5.3.5, Protein Metrics Inc.) with a UniProt human database (20,376 entries). The mass tolerance for precursors and fragment ions was set at 10 and 15 ppm, respectively. Cleavage sites were set as KR (C-terminal) and ST (N-terminal). Missed cleavages were set as 1. The fixed and variable modifications were carbamidomethylation (cysteine), and oxidation (methionine), respectively. In addition, the 78 O-linked and 309 N-linked glycan libraries of PMI-Byos were employed for intact O- and N-glycopeptides analysis with 1% false discovery rate (FDR) at peptide-spectrum-match (PSM) level. Strict quality control for intact O- and N-glycopeptide identification were carried out with scores higher than 200, and mass error less than 10 ppm.

QUANTIFICATION AND STATISTICAL ANALYSIS

Paired ratios from the same donor were compared using the nonparametric Wilcoxon signed-rank test. Ratios between two groups were compared using the Mann-Whitney U test. Student *t* test was used to compare luciferase intensity of tumors and the intensity of proliferation dyes. Statistical significance was set at a two-sided *p* level of 0.05. The levels of significance were denoted as follows: $*p < 0.05$; $**p < 0.01$; $***p < 0.001$.

ADDITIONAL RESOURCES

ClinicalTrials.gov identifier: NCT06014073.

CellPress
OPEN ACCESS

Supplemental figures

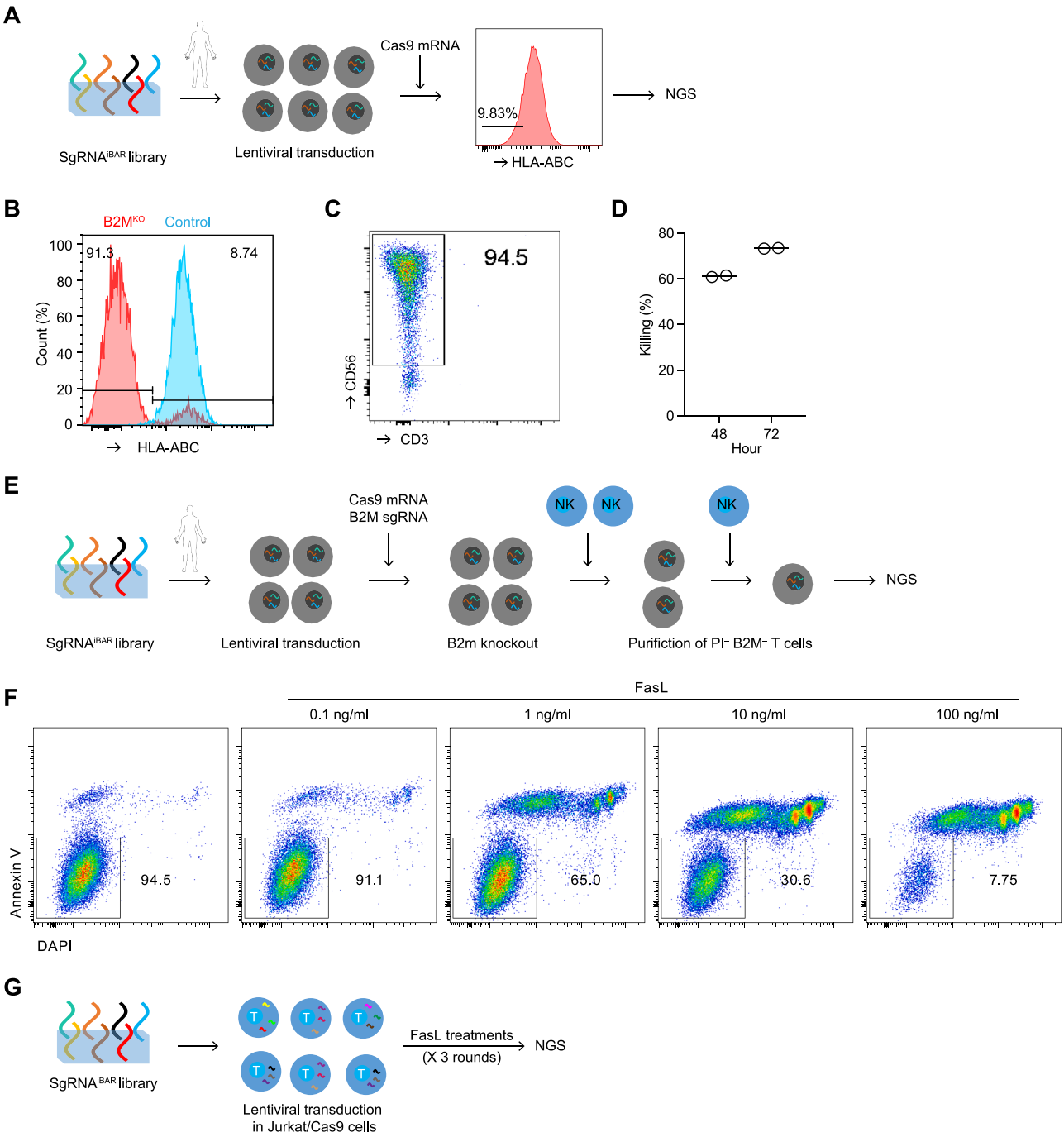

Figure S1. Setting of genome-wide CRISPR-Cas9 screenings, related to Figure 1

(A) Workflow of the whole-genome screening of HLA-ABC^{low} expression, which involved infecting T cells with lentiviral sgRNAs and treating them with Cas9-mRNA, fractionating HLA-ABC^{low}-expressing T cells, and sequencing.

(B) *B2M* knockout verification in primary T cells.

(C) Verification of the purity of isolated NK cells.

(D) Predetermination of NK cell-mediated killing toward primary *B2M*^{KO} T cells.

(legend continued on next page)

(E) Workflow of the whole-genome screening of NK cell-mediated killing. Primary T cells were infected with genome-wide lentiviral sgRNAs and electroporated with B2M sgRNA and Cas9 mRNA. The *B2M*-null T cell library was treated with 2-round purified primary NK cells and purified following $PI^{neg}B2M^{neg}$ strategy for further sequencing.

(F) Jurkat T cell viability under different doses of FasL.

(G) Workflow of the whole-genome screening of FasL killing, which involved treating Jurkat T cells three times with FasL.

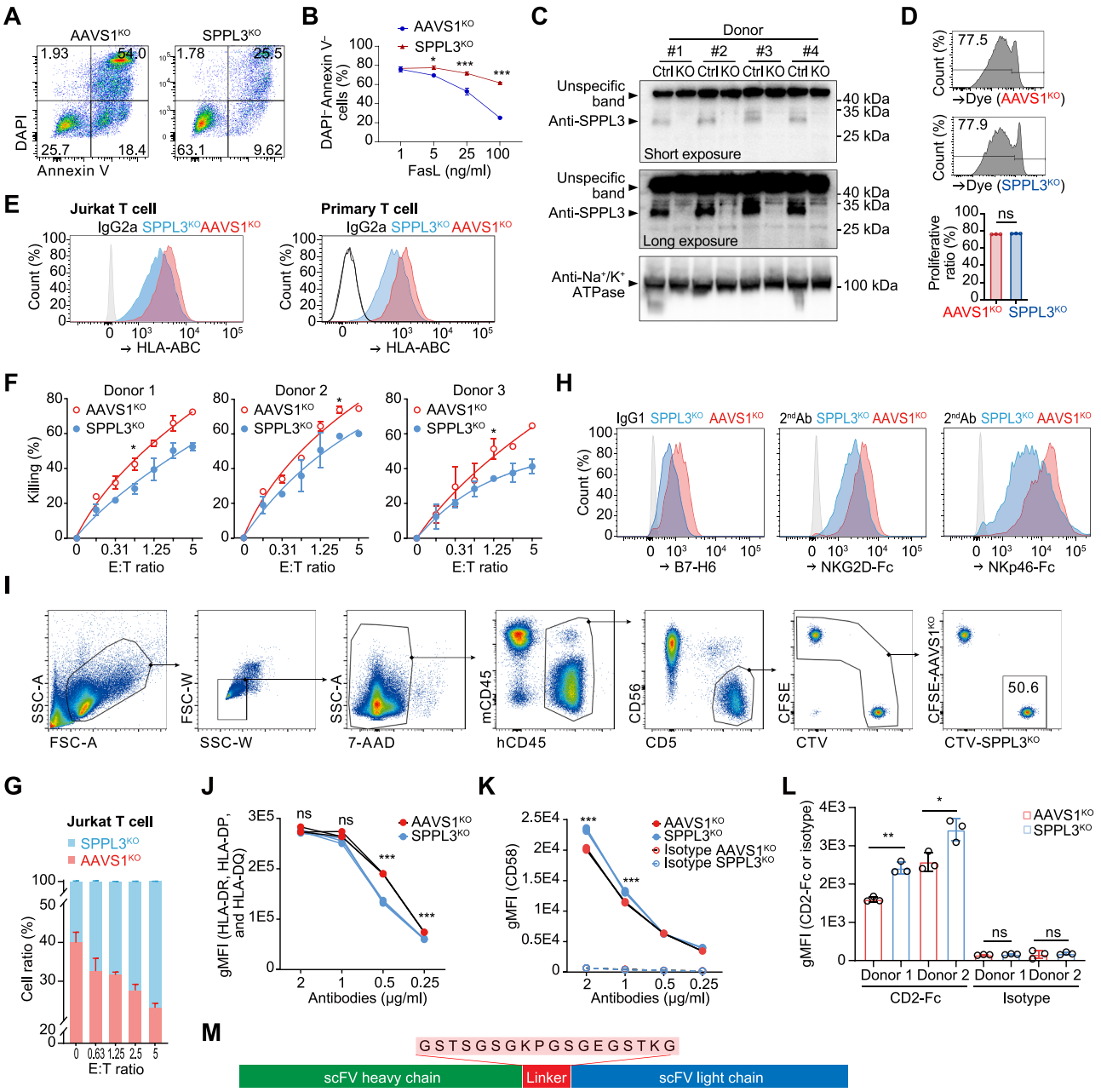

Figure S2. Characteristics of *SPPL3*^{KO} T cells, related to Figure 2

(A) Analysis of Jurkat T cell viability in the presence of 100 ng/mL FasL overnight. The plots are representative of three independent experiments.

(B) Dose-dependent killing of Jurkat T cells by FasL.

(C) Verification of *SPPL3* knockout efficiency in primary T cells.

(D) CFSE-labeled *SPPL3*^{KO} and *AAVS1*^{KO} T cells were cultured in equal numbers for 4 days and were FACS evaluated to assess proliferation based on CFSE level.

(E) Binding of anti-HLA-ABC monoclonal antibody on *SPPL3*^{KO} (blue) and *AAVS1*^{KO} (red) in Jurkat T cells (left) and human primary T cells (right), with isotype controls indicated as black or gray lines.

(F) Resistance of SPPL3-KO primary T cells to TCR-T cell killing. Target cells consisted of HLA-A2-positive T cells transduced with CTAG1B. Equal quantities of CTAG1B+/AAVS1^{KO} and CTAG1B+/SPPL3^{KO} T cells were combined and co-cultured with NY-ESO-1-specific TCR-T cells for a period of 24 h. To quantify absolute cell death, 5,000 absolute counting beads were introduced during flow cytometry acquisition to precisely determine the exact number of viable T cells of interest and subsequently compare these data to the untreated group.

(G) Evaluation of allogeneic NK cell killing against Jurkat T cells. *SPPL3*^{KO} cells were cultured with control cells (*AAVS1*^{KO}) and were either treated with purified NK cells or left untreated. The percentages of *SPPL3*^{KO} cells were measured by flow cytometry.

(legend continued on next page)

(H) Binding of anti-B7-H6, anti-NKG2D-Fc, and anti-NKp46-Fc antibodies on *SPPL3*^{KO} (blue) and *AAVS1*^{KO} (red) Jurkat T cells, with staining controls indicated as black lines.
(I) Flow cytometry analysis strategy of human T cells from NCG mice.
(J) Detection of HLA-II on T cells. A total of 0.2 million human T cells were diluted in 100 μL of staining buffer and incubated with the specified antibody concentrations at room temperature for 30 min.
(K) Detection of CD58 on T cells. A total of 0.2 million human T cells were diluted in 100 μL of staining buffer and incubated with the specified antibody concentrations at room temperature for 30 min.
(L) Binding of CD2-Fc on T cells.
(M) The linker information of anti-CD19 CAR.
The data presented are representative of three independent experiments (D–H) and two independent experiments using different donors (J–L). Horizontal lines indicate the mean. The data in (B) ($n = 3$), (D) ($n = 3$), and (F) ($n = 3$) are reported as means ± SDs. Mann-Whitney U test was performed for analysis. Data presented in (J)–(L) were analyzed using t test. $^{*}p < 0.05$, $^{**}p < 0.01$, $^{***}p < 0.001$.

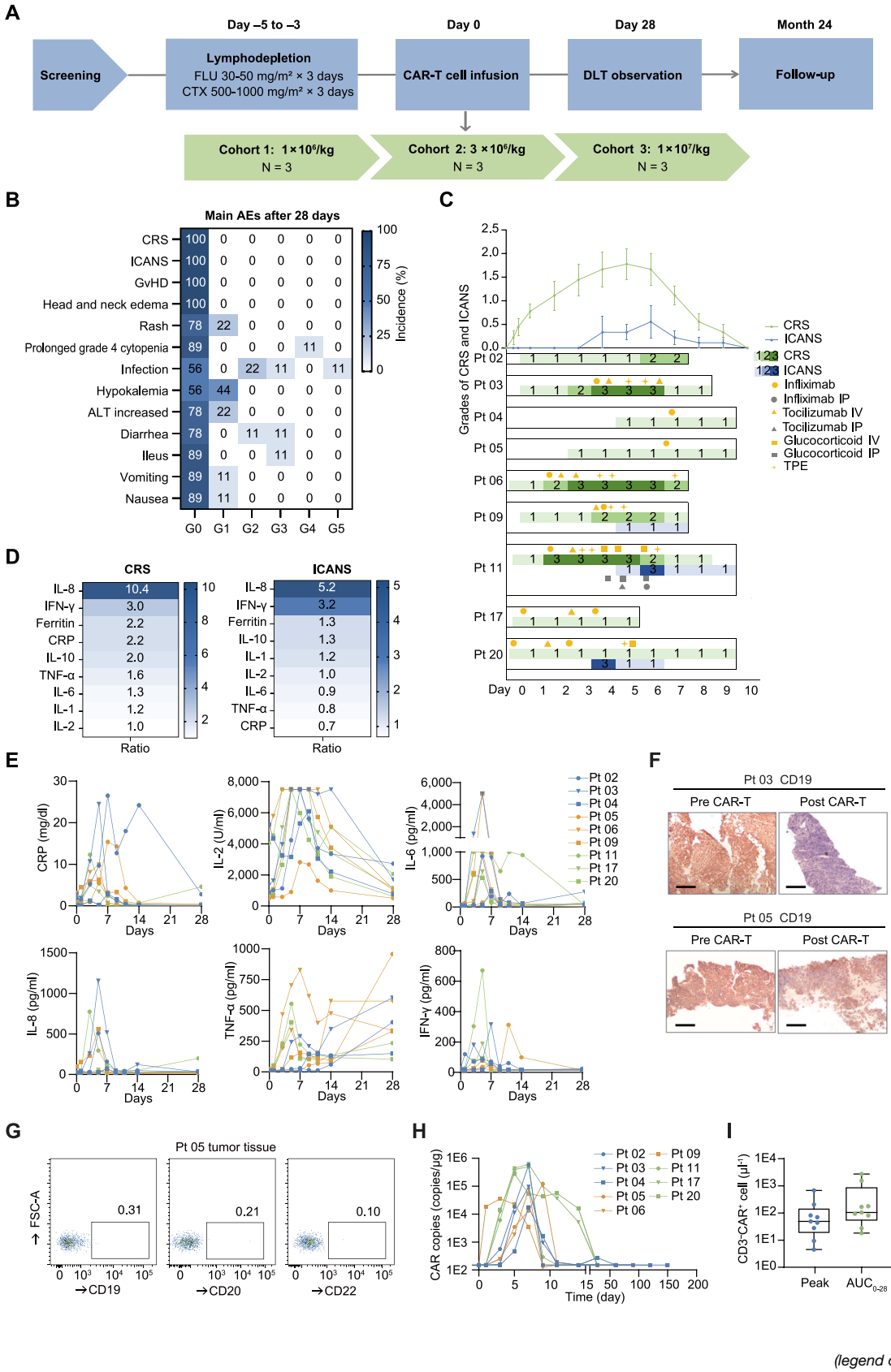

(legend on next page)

Figure S3. Flowchart, safety, and cytokine responses of the CAR-T therapy, related to Figure 5

(A) Flowchart illustrating the phase I study evaluating CAR-T therapy for relapsed/refractory B-NHL.

(B) Time-dependent grading of CRS and ICANS in patients (n = 9).

(C) Incidence and frequency of the main AEs observed after CAR-T therapy (n = 9). The interventions for the control of CRS were indicated.

(D) Cytokines associated with CRS (left) and neurologic events (right) are presented as median ratios based on the ratio of median peak levels in ≥grade 3 events to grade 2, grade 1, or no events. Color scales indicate the median ratio, with increasing intensity representing higher values.

(E) Changes in cytokine levels within 28 days after CAR-T infusion.

(F) Comparison of CD19 expression levels in tissue samples from Pts 03 and 05 before and after CAR-T therapy. Scale bar, 50 μm.

(G) Analyze the CD19, CD20, and CD22 expression levels in tissue sample from Pt 05 after CAR-T therapy.

(H) Quantification of CAR copies, measured as vector transgene copies per microgram of genomic DNA in peripheral blood samples.

(I) Peak and AUC_{0-28} of $CD3^{-}CAR^{+}$ cells in peripheral blood throughout the treatment duration.

Pt, patient; CRS, cytokine release syndrome; ICANS, immune effector cell-associated neurotoxicity syndrome; GvHD, graft-versus-host disease; ALT, alanine aminotransferase; i.v., intravenous injection; i.p., intraperitoneal injection; TPE, therapeutic plasma exchange.

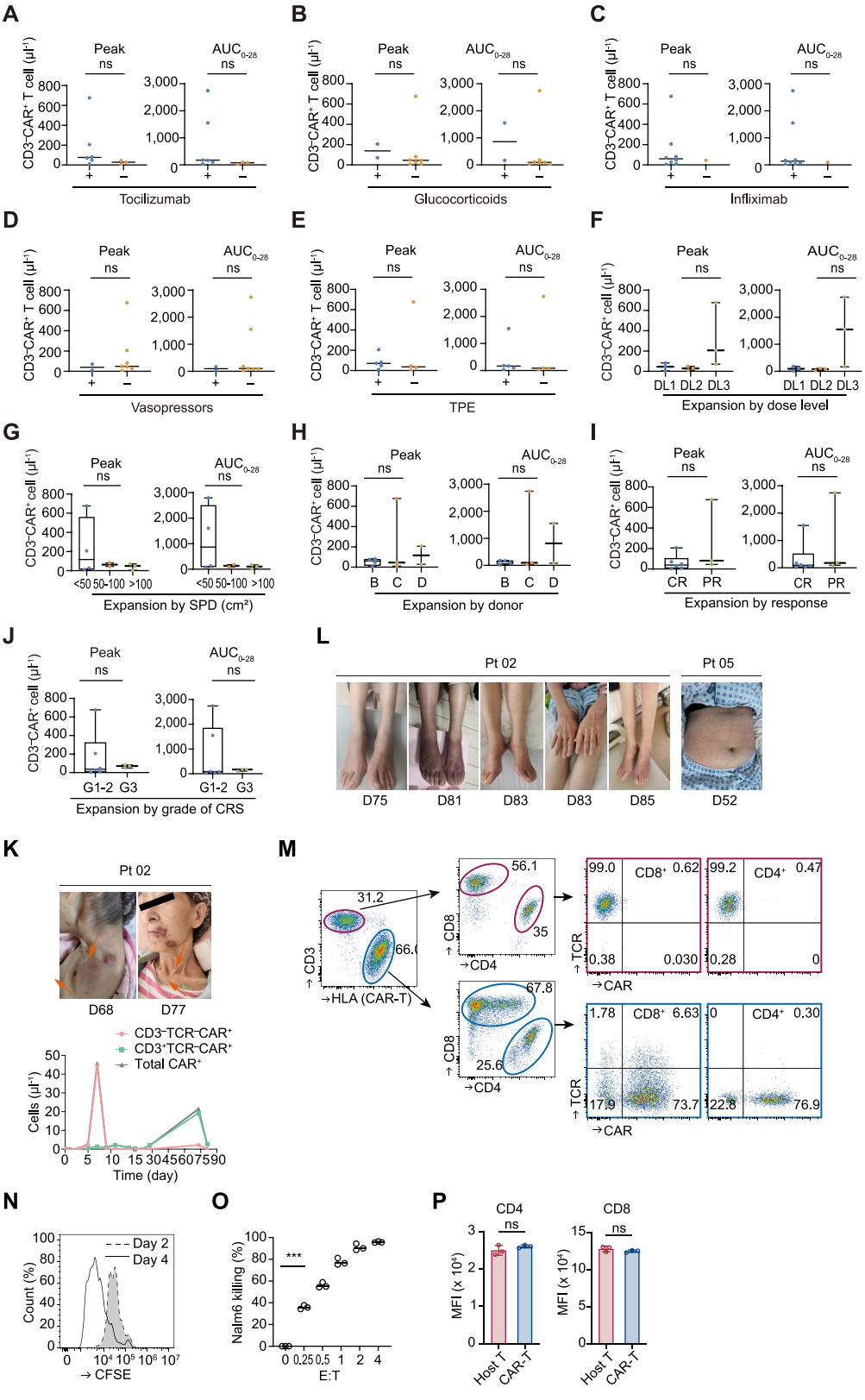

(legend on next page)

Figure S4. Evaluation of CAR-T cell expansion dynamics and clinical parameters in patient samples, related to Figure 5

(A–J) Comparison of CAR-T cell expansion metrics across interventions: tocilizumab (A), glucocorticoids (B), infliximab (C), vasopressors (D), and therapeutic plasma exchange (TPE) (E). Comparison of expansion peak and $AUC_{0\text{-}28}$ across different dose levels (F), tumor burden SPD ranges (G), different donors (H), responses (I), and CRS grades (J). DL, dose level; AUC, area under the curve; SPDs, the sum of product diameters; CR, complete response; PR, partial response. The data are reported as means ± SDs. Statistical analysis was performed using the t test, and "ns" indicates no significant differences.

(K) Clinical manifestation of neck mass and quantification of CAR-T cells in Pt 02, highlighting the expansion of $CD3^+TCR^+$CAR-T cells at a later time point.

(L) Skin manifestations observed in Pts 02 and 05 at specific days following CAR-T cell infusion.

(M) Identification and analysis of CAR-T cells in the peritoneal cavity on day 9 in Pt 11, with gating performed on live lymphocytes.

(N) Assessment of CAR-T cell proliferation from Pt 11 over a period of 2 and 4 days, with diluted dyes indicating proliferating cells.

(O) Evaluation of target cell killing by CAR-T cells isolated from ascites of Pt 11.

(P) Detection and comparison of indicated molecules on patient (host) T cells and CAR-T cells from ascites of Pt 11.

The data in (O) ($n = 3$) and (P) ($n = 3$) are reported as means ± SDs. Statistical analysis was performed using the t test in (O) and (P). ns indicates no significant differences; $^{***}p < 0.001$.

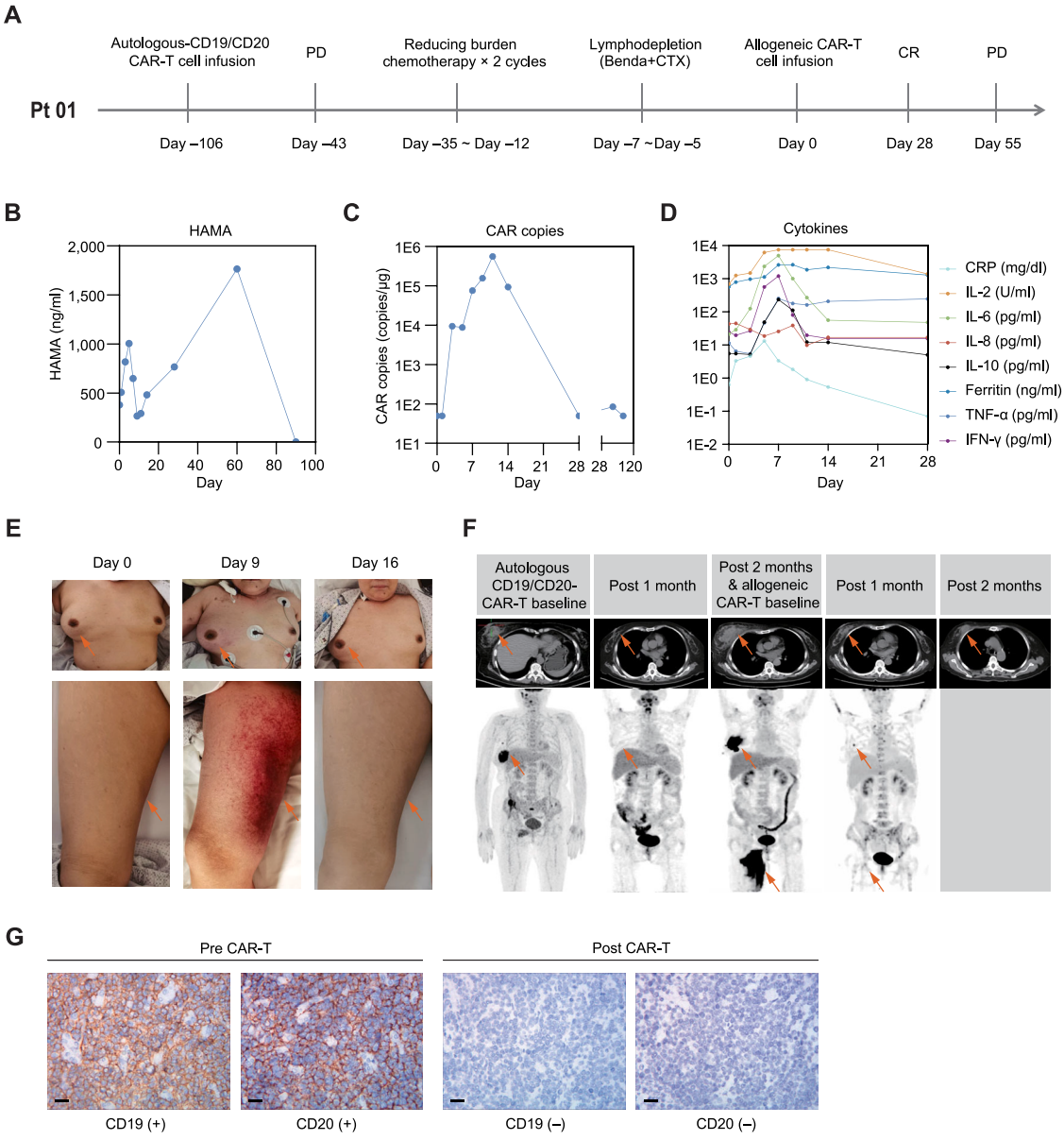

Figure S5. The clinical information and outcome of Patient 01 with CAR-T therapy, related to Figure 5

(A) Treatment course of the patient with previous autologous CD19/CD20 CAR-T cell therapy and *SPPL3*^{KO}/TCR^{KO} anti-CD19 CAR-T therapy.

(B) Detection of serum human anti-mouse antibodies (HAMAs).

(C) Quantitative PCR-based detection of CAR copy numbers after *SPPL3*^{KO}/TCR^{KO} anti-CD19 CAR-T infusion.

(D) Measurement of cytokine levels after *SPPL3*^{KO}/TCR^{KO} anti-CD19 CAR-T infusion.

(E) Skin changes in the right breast and right thigh tumor lesions during the treatment process.

(F) PET-CT and CT images, from left to right, showing the baseline images of autologous CD19/CD20 CAR-T cell therapy, 1 month after infusion, 2 months after infusion, or the baseline of *SPPL3*^{KO}/TCR^{KO} anti-CD19 CAR-T therapy, 1 month and 2 months after *SPPL3*^{KO}/TCR^{KO} anti-CD19 CAR-T cell infusion.

(G) Immunohistochemistry of the right breast tumor tissue before and 2 months after *SPPL3*^{KO}/TCR^{KO} anti-CD19 CAR-T therapy. Scale bar, 20 μm.

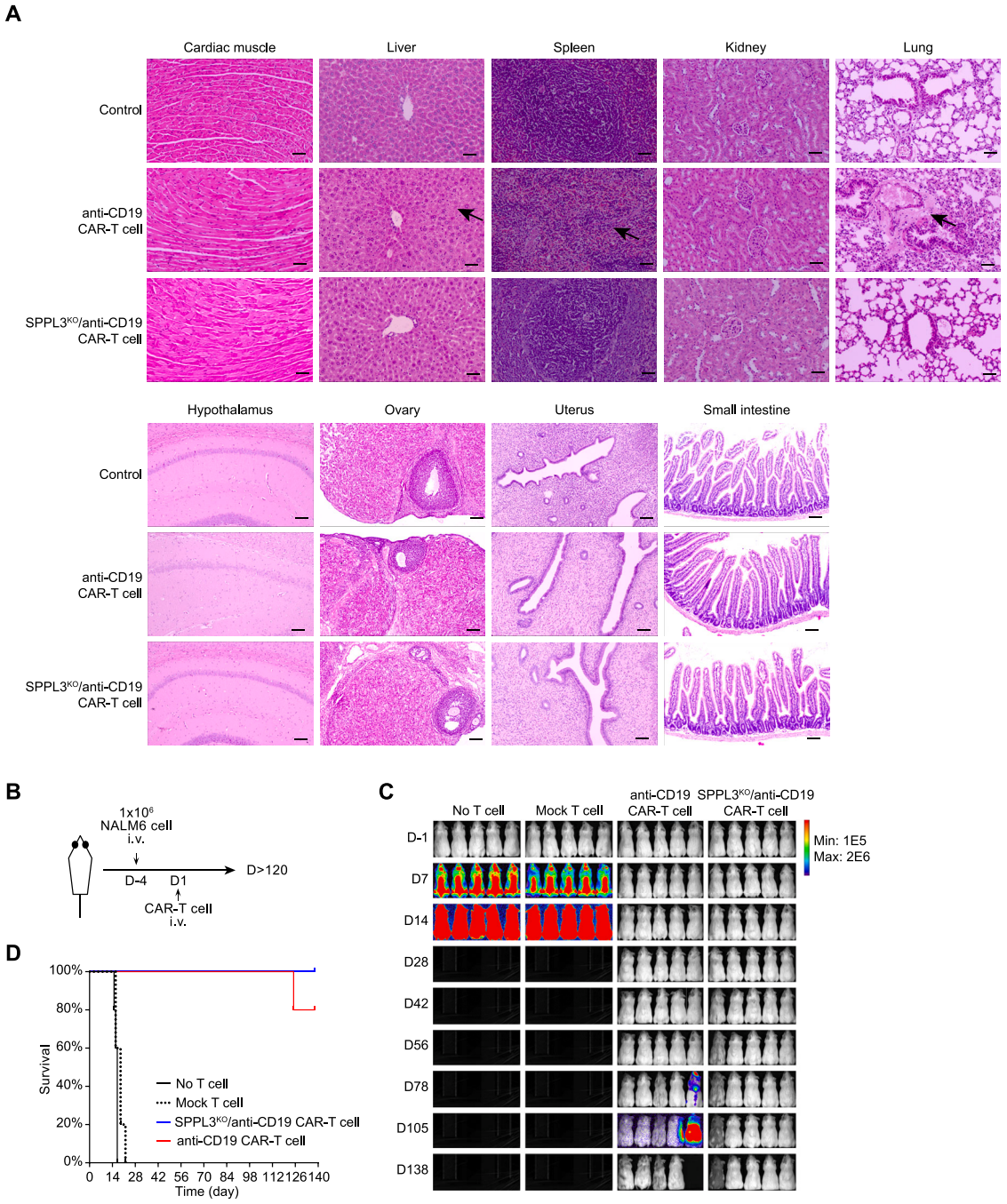

Figure S6. Histopathologic safety assessment and anti-tumor efficacy of SPPL3^{KO} anti-CD19 CAR-T cells, related to Figure 6

(A) Hematoxylin and eosin (H&E)-stained sections from six mice per group were evaluated across multiple organs, comparing control, wild-type CAR-T, and *SPPL3*^{KO} CAR-T groups. Lesions are indicated by arrows. Lesion incidence was observed as follows: cardiac tissue (0% versus 0% versus 0%), liver (0% versus 33.3% versus 16.6%), spleen (0% versus 66.6% versus 16.6%), kidney (0% versus 0% versus 0%), lung (0% versus 16.6% versus 0%), hypothalamus (0% versus 0% versus 0%), ovary (0% versus 0% versus 0%), uterus (0% versus 0% versus 0%), and small intestine (0% versus 0% versus 0%). Scale bars: 200 μm.

(B) Schematic representation of the experiment setup. The number of T cells is 1×10^7 per mouse.

(C) Bioluminescence imaging (BLI) images showing tumor burden ($n = 5$ per group).

(D) Kaplan-Meier plot showing the overall survival of all groups. No T cell group is indicated in the black line, and the mock T cell group is represented by the dashed line. The groups received *SPPL3*^{KO}/anti-CD19 CAR-T cells, and anti-CD19 CAR-T cells are represented by the blue and red lines.

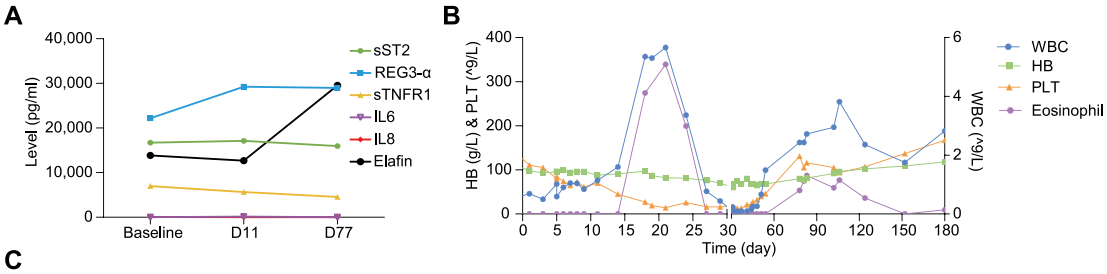

C

	A		B		C		DRB1		DQB1		DPB1	
Patient	A*31:01	A*31:01	B*15:18	B*40:02	C*03:04	C*07:04	8:02	11:01	3:01	3:02	2:02	4:02
Donor	A*02:01	A*30:01	B*13:02	B*15:18	C*06:02	C*08:01	4:04	7:01	2:02	3:02	4:02	17:01

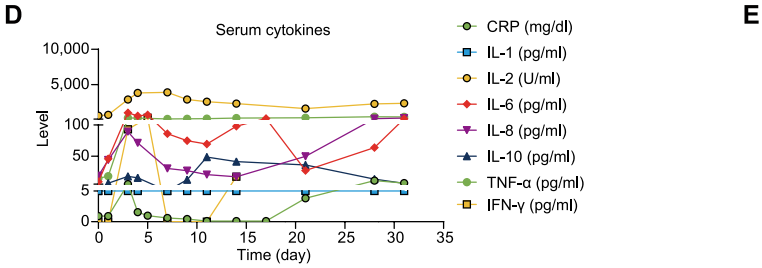

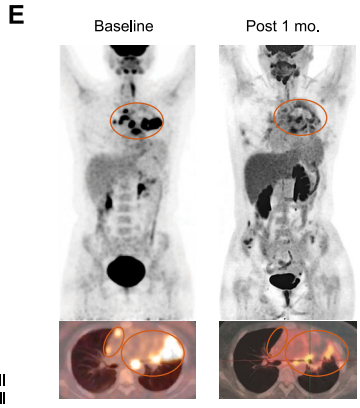

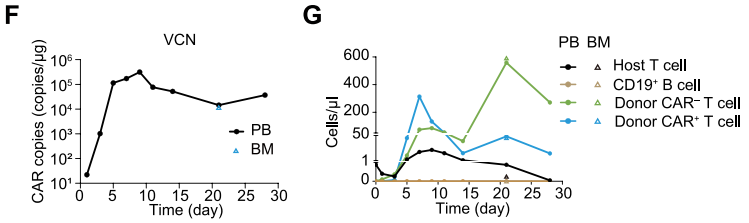

H

	A		B		C		DRB1		DQB1		DPB1	
Patient	A*03:01	A*11:01	B*15:01	B*35:03	C*04:01	C*04:01	9:01	13:01	6:03	3:03	2:01	4:01
Donor	A*02:01	A*30:01	B*13:02	B*15:18	C*06:02	C*08:01	4:04	7:01	2:02	3:02	4:02	17:01

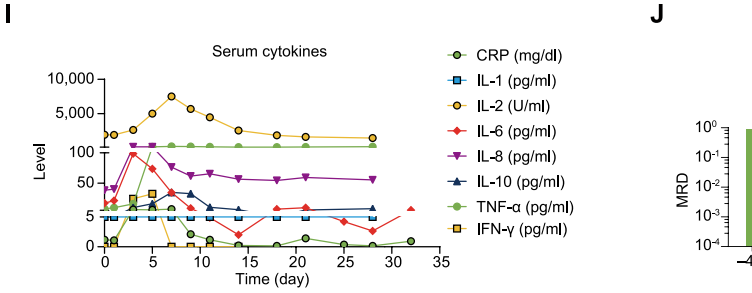

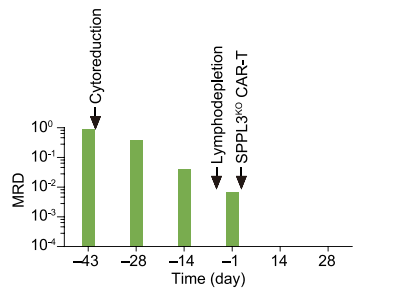

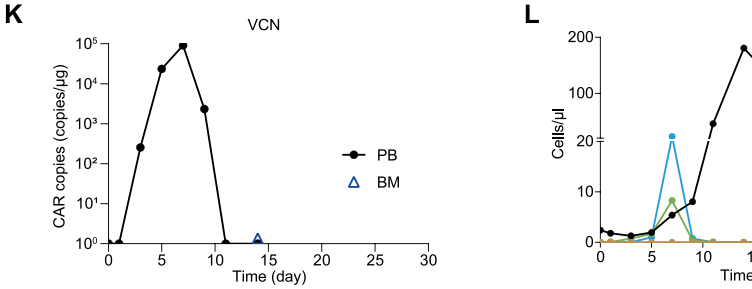

(legend on next page)

Figure S7. Clinical characteristics and outcomes of patients receiving TCR-sufficient anti-CD19 CAR-T cells, related to Figure 7

(A) Detection of GvHD markers at various time points.
(B) Kinetics of the indicated cell types.
(C) HLA information of the donor and recipient.
(D) Serum cytokine concentrations during CAR-T therapy.
(E) PET-CT scans of pre-infusion at 1 month post-CAR-T infusion.
(F) Quantification of CAR copies in peripheral blood and marrow.
(G) Monitoring the expansion of host T cells, donor T cells, and B cells in peripheral blood over time, with additional marrow analysis at day 21.
(H) HLA typing of the donor and recipient.
(I) Serum cytokine concentrations measured during CAR-T therapy.
(J) Minimal residual disease (MRD) levels detected by flow cytometry at various time points, with key treatment dates indicated by arrows.
(K) Quantification of CAR copy numbers in peripheral blood, with additional marrow analysis at day 14.
(L) Kinetics of the indicated cell types over time.